

**INVESTIGATION OF SKIN DOSE IN MEGAVOLTAGE RADIATION THERAPY FOR
BREAST CANCER**

by

Yasmeen Khan

B.Sc., Umm Al Qura University, 2009

A THESIS SUBMITTED IN PARTIAL FULFILLMENT OF
THE REQUIREMENTS FOR THE

MASTER OF SCIENCE

in

**The Faculty of Graduate Studies and Postdoctoral Studies
(Physics)**

THE UNIVERSITY OF BRITISH COLUMBIA

(Vancouver)

March 2017

© Yasmeen Khan, 2017

Abstract

Dermatitis and skin reactions are frequently associated with whole breast radiotherapy (WBRT). The severity of the skin damage depends on many factors such as x-ray beam energy, radiation therapy technique, breast size and shape, existence of skin folds, total radiation dose and dose per fraction. Dermatitis can vary from dryness to a severe skin reaction such as moist desquamation or ulceration. Radiation dermatitis may affect the quality of life or treatment outcome in extreme cases. The most severe skin reactions generally occur in skin folds due to dose buildup effects in megavoltage photon beams. Although modern radiation therapy techniques have been shown to reduce skin dose, in some patients, the skin still receives a higher radiation dose than necessary. Better positioning during radiation therapy to reduce skin folds may provide further reduction in unnecessary skin dose. Furthermore, better breast positioning may also lead to reduction in the volume of normal tissues irradiated, further benefitting the patient.

This thesis is an investigation of the impact of breast position on radiation dosimetry at the skin surface in megavoltage x-ray beams for intensity modulated radiation therapy. Radiological properties of potential materials for construction of a breast positioning device are studied.

Preface

All exertions of this dissertation were conducted at the BC Cancer Agency, Vancouver center. I wrote the manuscript, performed the data collection and analysis for Chapters one, two and three. The data in Chapters four and five were acquired with the assistance of Joel Beaudry, MSc. I performed the primary data analysis as well as the manuscript composition in these chapters. Chapter 6 was written by me and the future work described relates to that of the breast device development team including therapists, engineers, and physicists at the BC Cancer Agency Dr. Cheryl Duzenli was involved throughout the project as the supervisor and manuscript reviewer.

Table of Contents

Abstract	ii
Preface	iii
Table of Contents.....	iv
List of Tables	vii
List of Figures	viii
List of Abbreviations	x
Acknowledgements	xii
Dedication.....	xiii
Chapter 1: Introduction	1
1.1 Breast cancer.....	1
1.2 Breast cancer treatment.....	1
1.3 Radiation therapy for breast cancer.....	2
1.4 Radiation to skin.....	3
1.4.1 Basic skin biology.....	3
1.4.2 Radiation dose in the skin region.....	4
1.5 Breast positioning.....	7
1.6 Current status of breast positioning.....	8
1.7 The aim of this thesis	12
Chapter 2: Surface dose in megavoltage x-ray beams.....	18
2.1 Introduction.....	18
2.1.1 Linear accelerator	18
2.1.2 Eclipse™ treatment planning system.....	19
2.1.3 Factors impacting surface dose.....	20
2.1.3.1 Energy.....	20

2.1.3.2 Field size	21
2.1.3.3 Obliquity	21
2.1.3.4 Source to surface distance (SSD)	22
2.2 Surface dose calculations in the Eclipse™ treatment planning system	22
2.2.1. Demonstration of entrance and exit skin dose for a simple geometric phantom	23
2.3 Conclusion	25

**Chapter3: Improving surface dose in skin folds during breast radiotherapy by
modifying breast position 34**

3.1 Introduction.....	34
3.2 Background.....	34
3.2.1 Contouring.....	34
3.1.2 Tangent fields' set-up	35
3.1.3 IMRT treatment planning technique	36
3.2 Materials and methods.....	37
3.2.1 Treatment planning.....	37
3.2.2 Measurements	40
3.3 Results and discussion:	41
3.4 Conclusion	44

Chapter 4: Film dosimetry for breast surface dose 54

4.1 Introduction.....	54
4.2 Method and materials.....	54
4.2.1 CT and treatment planning calculation	54
4.2.2 Film calibration	55
4.2.3 Breast phantom dose delivery.....	55
4.2.4 Film analysis	56
4.3 Results and discussion:	57

4.5 Conclusion.....	59
Chapter 5: Radiological properties for breast immobilization devices.....	74
5.1 Introduction.....	74
5.2 Methods and materials.....	75
5.2.1 Dose buildup curves: Marcus ionization chamber	75
5.2.2 Radiochromic film dosimetry for Carbon fibre sheet	76
5.3 Results.....	76
5.3.1 Dose buildup using Marcus ionization chamber	76
5.3.2 Radiochromic film dosimetry for Carbon fibre sheet	77
5.4 Discussion.....	78
5.4 Conclusion.....	79
Chapter 6: Conclusion and future work	84
6.1 Conclusions.....	84
6.2 Future work.....	84
References	85

List of Tables

Table 1.1: A summary of different immobilization	17
Table 3.1: V100%BS.	53
Table 3.2: V100%SF and skin fold volume.	53
Table 4.1: Point's dose calculated by Eclipse TPS.....	73

List of Figures

Figure 1.1: Schematic diagram of human skin.....	14
Figure 1.2: Kerma and absorbed dose curves.....	15
Figure 1.3: Breast patient treatment position.	16
Figure 2.1: A schematic diagram of linear accelerator components in photon beam mode.	26
Figure 2.2: The percentage depth dose vs. energy.	27
Figure 2.3: The percentage depth dose vs. field size.	28
Figure 2.4: The dose distribution with different beam incident angle.....	29
Figure 2.5: The percentage depth dose vs. beam incident angle.....	30
Figure 2.6: Validation curve for Eclipse data with Marcus ionization chamber data.	31
Figure 2.7: Schematic of field's arrangement to determine the dose in region of interest (ROI) for cuboid phantom thickness (t).....	32
Figure 2.8: Surface dose vs. cuboid phantom thickness (I).	33
Figure 3.1: The inferior skin fold and Styrofoam wedge effect in sagittal view.....	45
Figure 3.2: The lateral skin fold in another patient.	46
Figure 3.3: Target and organs at risk contours.	47
Figure 3.4: Modified breast contours.....	48
Figure 3.5: whole body skin contour , PROI, and Skin fold contour.....	49
Figure 3.6: Skin dose vs. separation (II).....	49
Figure 3.7 (a-d): Variation in treatment parameters generated by Styrofoam wedge, without Styrofoam wedge, and modified breast.	51
Figure 4.1: EBT3 film calibration set up.....	61

Figure 4.2: Phantom without Styrofoam wedge set up for dose delivery.	62
Figure 4.3: Phantom with Styrofoam wedge set up for dose delivery.	63
Figure 4.4: Film calibration curve in red channel.	64
Figure 4.5: EBT3 film validation curve with Marcus ionization chamber data.....	65
Figure 4.6: Representation of measurements for films placed on the breast and chest surfaces.....	66
Figure 4.7: Measured dose profiles for without and with Styrofoam wedge.	67
Figure 4.8: The difference in the dose distribution and water bag shape in without and with foam wedge plans in the sagittal view.	68
Figure 4.9: Entrance and exit films measurements on the breast surface.	69
Figure 4.10: Total doses from entrance and exit in beams on the medial and lateral breast surface.....	70
Figure 4.11: Skin dose vs. separation (III).....	71
Figure 4.12: Cross sectional view of dose distribution and dose points.	72
Figure 5.1 (a-c): Marcus ionization chamber measurement set up. Error! Bookmark not defined.	
Figure 5.2: Percentage depth dose curves using Marcus ionization chamber for 6 MV photon beam.....	81
Figure 5.3: Percentage depth dose curves using Marcus ionization chamber for 10 MV photon beam.....	82
Figure 5.4: The variation of dose profiles for one-seven carbon fiber sheets measured by EBT3 films.	83

List of Abbreviations

AAA	an anisotropic analytical algorithm
BCCA	British Columbia Cancer Agency
BCS	breast conserving surgery
CT	Computed Tomography
CTV	Clinical Target Volume
DVH	Dose Volume Histogram
EBRT	External Beam Radiotherapy
F.Z	Field size
GTV	Tumor Target Volume
ICRU	International Commission on Radiation Units and Measurements
IMRT	Intensity-modulated Radiotherapy
MLC	Multi Leaf Collimator
MRI	magnetic resonance imaging
MV	Mega Voltage
OAR	Organ at Risk
PBC	pencil beam Convolution
PROI	Patient region of interest
PTV	Planning Target Volume
PVC	polyvinylchloride
ROI	Region of interest
SAD	Source Isocenter Distance

SSD	Source Isocenter Distance
TNM	Tumor, lymph node, and metastases
TPS	Treatment Planning System
US	Ultra Sound
Z	atomic number
3D-CRT	Three Dimensions- Conformal Radiotherapy

Acknowledgements

I would like to address my great appreciation and thanks to my research supervisor Dr. Cheryl Duzenli for her support and assistance throughout the completion of my studies and research. I am sincerely thankful for her comments and valuable feedback during my study process. She always welcomed any questions or consultations, and she is incredible source of supervision and support. I have had helpful discussions and questions with her. I will not forget her encouragement, advices, and support.

I would like to acknowledge Joel Beaudry for his efforts and assistance in this project and I also thank him for providing me with his Marcus ionization chamber validation data. In addition, I would also like to extend my gratitude to members of Physics at the BC Cancer Agency Vancouver Center for their help in this work particularly Dr. Steven Thomas, and Dr. Fred Cao, for expertise with Eclipse™ and IMRT technique. I also must extend my thanks to the radiation therapists and dosimetrists at Radiation Therapy Department in Vancouver Centre.

I would like to express my appreciation and thanks to my parents, siblings, and my entire extended family and friends for their continued support of my education and research. Great appreciation is provided to my husband Saud for his encourage and support. Additionally, I would like to thank Dr. Abdul Hamid Saudi, Dr. Noor Mail and Dr. Ramani Ramaseshan for their encouragement and support.

Dedication

To my family and husband

Chapter 1: Introduction

1.1 Breast cancer

Breast cancer is the most commonly diagnosed type of cancer (Manoharan & Pugalendhi, 2010). Predominantly older women are affected by breast cancer, but it can also affect younger women. It has recently been estimated in Canada that breast cancer accounts for 26% of all new cancer cases. Moreover, breast cancer deaths accounted for 14% of all cancer deaths in women (Breast Cancer in Canada, 2015). The annual incidence of breast cancer is 100 cases per 100,000 people, as reported by Canadian Cancer Society. In British Columbia alone, 3,200 women were diagnosed with breast cancer in 2014 (Breast Cancer Society of Canada - statistics, 2015).

1.2 Breast cancer treatment

Breast cancer staging is described by the TNM system that provides information about the tumor size (T) and degree of loco-regional invasion of nodal regions (N), and the degree of spread to distance metastasis (M). Breast cancer staging is assessed by clinicians using different imaging modalities such as ultra sound (US), magnetic resonance imaging (MRI,) and mammography.

Breast cancer treatment options depend on tumor stage, size, the extent of spread, as well as patient's pathology report (Siegel, Miller, & Jemal, 2015). Breast cancer can be treated effectively by one or a combination of the following options: surgery, radiation

drugs (chemotherapy and hormonal therapy), and targeted therapies (immune therapies) (Martincich, Bertotto, & Montemurro, 2012; Siegel, Miller, & Jemal, 2015).

Historically, surgical treatment was aggressive with the goal to remove as much of the breast and surrounding area as feasible (Torre et al., 2015). Mastectomy, representing one type of surgery, consists of removing the whole breast (Chen, Gilkeson, & Fei, 2007; Peart, 2015). Another type of surgery called lumpectomy or 'breast conserving surgery (BCS)' consists of removing the tumor and a margin around it instead of removing the entire breast (Peart, 2015; Breast Cancer Statistics - Canadian Cancer Society, 2015).

Regularly, breast conserving surgery is followed by either 6 or 7 weeks of radiation therapy to make sure that no tumor cells remain, or, by chemotherapy in order to control the extent of spread of cancer cells, or both (Peart, 2015; Breast Cancer Statistics - Canadian Cancer Society, 2015). Adjuvant external beam radiotherapy is the treatment of choice to enhance local control and survival for patients with high-risk breast cancer and mastectomy. In addition, it is preferable for T1, T2, and T3 tumors, as breast conservation therapy (Sun et al., 2014).

1.3 Radiation therapy for breast cancer

The general objective of radiotherapy is to deliver a lethal dose to the tumor while delivering minimal exposure to surrounding normal tissues (López et al., 2002). Radiation therapy after breast conserving surgery reduces the cancer recurrence rate by half, and the death rate by one sixth (Gray, R., Early Breast Canc Trialists Collab, & Early Breast Cancer Trialists' Collaborative Group (EBCTCG), 2011).

There are two types of radiotherapy; external or internal. External radiotherapy (ERT) is usually given once a day for a period of 4-7 weeks for a total of 16-28 fractions to the whole breast and often with an extra 4-8 fraction to the tumor bed. External beams of high energy photons are used to deliver the radiation dose. The total dose of radiation to be given is decided by the oncologist whereas the medical physicist and dosimetrist plan how that dose should be delivered using the current technology. Internal radiotherapy, known as brachytherapy uses radioactive materials implanted into the tissue. This thesis focuses on external beam treatment only.

Although patients do not feel anything when the radiation beam is on, an adverse reaction to radiation can happen during the later stages of, or following treatment (Moody et al., 1994). Reactions can be either early (acute) or late. One such adverse reaction involves skin and underlying tissue damage.

The focus of this thesis is to investigate the underlying physics principles that relate to radiation dose to skin during radiotherapy for breast cancer in order to better understand how to reduce the incidence of acute skin reactions.

1.4 Radiation to skin

1.4.1 Basic skin biology

It is important to have a basic knowledge of skin biology in order to understand radiation skin reactions. A schematic diagram of human skin is shown in figure 1.1. The skin consists of two main layers, namely, the epidermis (superficial layer), and the dermis (deep layer). Between the epidermis and dermis, the basal layer is located. The basal layer

produces epidermal cells. Melanocytes are located between the basal cells. The pigment of the skin is produced by the melanocytes (Hopewell, 1990; Von Essen, 1969).

Repopulation of the epidermis by the basal layer is essential to the integrity of the skin. Ionizing radiation destroys stem cells in the basal layer and inhibits cell division. The rate of survival of basal cells in the epidermis will determine the degree of skin damage due to the radiation (Hopewell, 1990). Furthermore, skin reactions may be affected by other factors (Kraus-Tiefenbacher, 2012; Von Essen, 1969) such as age, other skin conditions, medical history, and chemotherapy (Gray, J. R. et al, 1991). Acute skin toxicity in breast cancer patients also depends on factors such as breast volume, T stage, allergies, smoking, hormone therapy, and radiotherapy technique (Kelly et al., 2011; Kraus-Tiefenbacher, 2012). Consequently, skin reactions vary among patients.

Acute skin toxicity can show up as erythema (skin reddening) and desquamation (loss of epidermal cells). Furthermore, desquamation can be dry or moist (Salvo et al., 2010). Using the scoring system Common Terminology Criteria for Adverse Events (CTCAE version 3.0), grades one, two and three are defined respectively as : 1) mild erythema or dry desquamation; 2) moderate to brisk erythema or patchy moist desquamation; and 3) confluent moist desquamation (De Langhe et al., 2014).

1.4.2 Radiation dose in the skin region

Modern radiation therapy uses high energy, mega voltage (MV) x-rays because they provide some skin sparing as a result of the dose build up effect. Skin sparing and dose build-up are related to the manner in which x-rays transfer energy to electrons and how electrons deposit energy, as described by the concepts of kerma and absorbed dose. Kerma

is kinetic energy released in the medium by energy transfer from photons to electrons. The electrons set in motion then dissipate their energy as radiation dose as they move through the medium. The dose is defined as energy absorbed per unit mass of the medium and the unit of dose is the Gray (Gy), in units J/kg. Kerma and dose for a mega voltage x-ray beam are illustrated in figure 1.2.

Electrons set in motion by high energy photons move primarily in the forward direction. Due to the increasing number of electrons set in motion with depth the number of electron tracks crossing the surface layer is smaller than at subsequent deeper layers in an absorbing medium. This is known as electronic disequilibrium. With increasing depth, the dose build-up region will be established as a result of an increasing number of electrons depositing dose (Johns & Cunningham, 1983, p 221-222). The number of electrons set in motion increases with depth until reaching the depth of maximum dose, coincident with the range of the electrons, where transient electronic equilibrium exists. Kerma, however, decreases constantly with increasing the depth as the x-rays are attenuated. Beyond the maximum dose, both Kerma and dose decrease with the increase in depth because of the photon attenuation.

The depth of maximum dose increases with increasing x-ray beam energy. The maximum dose may occur on the skin if superficial or orthovoltage (kilo-voltage) x-rays are used for treatment. In contrast in megavoltage x-ray beams, the maximum dose may occur more than 1 cm below the surface. The surface dose may be substantially less than the maximum dose (Almberg, Lindmo, & Frengen, 2011). For instance, 58.5% of the maximum dose is deposited in the first two millimeters of tissue when using 6 MV (Johns & Cunningham, 1983, p 746).

A confounding problem in radiation therapy for breast cancer is the existence of skin folds for some patients. As a result of skin folds skin sparing is lost as the skin can be beneath a layer of tissue and thus in a high dose region. The resulting high dose to the skin can cause a skin reaction such as moist desquamation (Barrett, Dobbs, Stephen, & Tom, 2009, p 269). Skin reaction occurrences may be more likely in breast radiotherapy compared with some other treatment sites due to skin folds.

Moreover, in breast radiation therapy, radiation beams are generally tangential to the skin surface (to be discussed later, section 2.). This can increase the surface dose and decrease the depth of maximum dose. An increase in the beam incident angle causes an increase in skin dose due to the obliquity of the photon path in medium (Metcalfe, Kron, & Hoban, 2004, p 243-244). Thus skin sparing is reduced.

Furthermore, the actual surface dose is increased by electron contamination from the beam source and backscattered radiation from the medium. Electron contamination exists in all x-ray beams. These electrons are caused by photon interactions in the air, machine head, or other materials in the path of the beam such as the flattening filter, collimator, and blocking tray (O'Shea & McCavana, 2003). The quantity of dose from electron contamination depends on the following factors: photon energy, field size, SSD (skin surface distance), beam modifiers such as multi-leaf collimator (MLC) or blocks, and obliquity of incidence (Khan, 2003, p 279-280).

In order to understand the risk of skin reaction, skin dose must be known accurately. It has been stated in the literature (Klein & Purdy, 1993; O'Shea & McCavana, 2003) that the measurement of the skin dose is challenging for the following reasons:

1- Shallow depth: 0.07 mm depth represents the typical depth of the basal layer, and the International Commission on Radiological Protection (ICRP) recommends measuring the skin dose at this depth (ICRP (International Commission on Radiological Protection), 1992; Orton & Seibert, 1972; Quach, Morales, Butson, Rosenfeld, & Metcalfe, 2000).

2-The skin falls within the high dose gradient region.

3- Charged practical equilibrium does not exist.

1.5 Breast positioning

Patient positioning has been identified as an important aspect of patient care in terms of accurate radiotherapy delivery. Patient positioning can also have an important impact on the presence of skin folds and hence skin dose. During breast radiation therapy, the patient generally lays in a supine position. The breast itself can be somewhat mobile and skin folds can be formed as a result of gravity, particularly for women with large or pendulous breasts. The most common immobilization device used for breast cancer patients in the supine position is the breast board. An example of a patient positioned with both arms up for breast radiation therapy is shown in figure 1.3.

The role of the breast-board device is to secure one or both arms above the head, as this lifts the breast superiorly, reducing breast sag. Cardiac doses may also be reduced in this position, and having both arms up provides symmetry if contralateral breast irradiation is required later. For additional patient comfort, a headrest, elbow, knee supports and a footboard are often provided.

Positioning can have an impact on quality of radiation therapy for breast cancer in two primary areas: dose optimization for tumor and organs at risk, and reproducibility. One of the organs at risk is skin as describe above. Good breast positioning should result in the elimination of skin folds. In addition, the use of immobilization devices should produce more stability, minimize the margins around the target and improve target coverage which could increase tumor control probability (Verhey, 1995).

1.6 Current status of breast positioning

Different techniques have been documented in the literature for the immobilization of breast cancer patients, particularly those with large or pendulous breasts. The following section attempts to represent the variety of immobilization techniques which exist for patients in the supine position. Table 1 shows a summary of different immobilization techniques described by various investigators. This selection of seven studies spanning the last 25 years is described in more detail below.

An early study by Cross et al. (Cross, Elson, & Aron, 1989) was conducted on four women having breast cup size EE. Patients were positioned in a modified lateral decubitus (angled to one side) position, treated with two tangent fields, using a 4MV photon beam. These patients were immobilized using customized Styrofoam support to position the breast. At the end of treatment, all studied patients presented moist desquamation in the infra-mammary fold. Moreover, it was stated that the surface dose in the presence of Styrofoam increased from 40% to 80%. However the measurement technique was not well described. Low beam energy and lack of modern delivery technology contributed to high skin doses in the study.

A report conducted by Bentel and Marks (Bentel & Marks, 1994) investigated a ring made of reinforced polyvinylchloride (PVC) tube to reposition large pendulous breasts on the chest wall and to reduce skin folds. 12 patients were treated with a customized ring device and strap fixed around the patient body, applying 6 MV x-rays beam dose with two tangent fields. They stated that the device not only reduced the skin fold, but also that it is easy to use with acceptable reproducibility. As additional benefit of using the ring device, they found an improvement in dose uniformity and a significant dose reduction in exposed lung by comparing 2D plans. The main breast ring disadvantage is the skin reaction. All patients treated with the device demonstrated a small area of moist desquamation in the inframammary fold area. The specific cause of the skin reaction was not determined but it was suggested that these complications could be due to the lack of modern delivery technique and low beam energy

Bentel et al. (Bentel, Marks, Whiddon, & Prosnitz, 1999) performed a follow up study in 1999 in 56 cancer patients using the PVC device mentioned above. Patients were again treated by using opposed tangential 6 MV photon fields and to improve the homogeneity of the dose, wedges or custom designed compensators were utilized. The ring positioning device was designed to reduce the skin fold. The correlation of skin reaction with breast's size and patient's weight was evaluated. The results showed that using the ring on the 56 patients raised the surface dose to 85% of the maximum dose, while in an open field without the ring; surface dose was 35% of d_{max} . Moreover, the surface dose on the phantom by utilizing the ring device increased up to 85% of d_{max} . 60.7% (34/56) of the patients who were treated with the ring positioning device developed moist desquamation in the inframammary fold and the others had erythema or hyperpigmentation. The results further

indicated that the patient's weight did not have any association with incidence of moist desquamation. It was concluded that these reactions could be related to the bolus effect that caused by the breast positioning ring.

Zierhut et al., (Zierhut, Flentje, Frank, Oetzel, & Wannemacher, 1994) published an investigation of the effect of utilizing a thermoplastic immobilization device on the skin dose. The experiments were performed with and without the immobilization in seven large pendulous breast cancer patients. All patients were treated by 6 MV photon beams and two tangent fields. Using thermoluminescent dosimeters (TLD), the results showed that the surface dose increased by almost 17% (from 47% to 64%) with the device in place. These measurements, which were repeated on the phantom, confirmed a similar effect (from 51% to 64%). The results also indicated that up to 86% of the studied cases developed erythema, whereas 14% had moist desquamation in inframammary folds areas. Hence, thermoplastic immobilization can raise the surface dose due to a bolus effect.

A pilot study of 8 cancer patients with large pendulous breasts was done by Latimer et al. in 2005 (Latimer, 2005). In this study, an in-house micro shell device was designed in a horse-shoe shape to minimize the skin fold, and hence reduce the severity of skin reaction. The ring device was formed around a plaster mould using a sheet of thermoplastic material. From breast phantom measurements, the use of the micro-shell produced higher skin dose by 9% compared with no device. Additionally, comparing with other devices tested in the study, the micro-shell caused the least increase in the surface dose (versus plastic tube and 14 mm garden hose) hence it caused the least skin reaction. After establishing the agreement between the clinical measurements and phantom measurements, they used the micro-shell device for all patients with large breasts who

have the tendency toward having skin folds. This study demonstrated the best result in terms of the skin dose however they did not quantify other treatment parameters and they only published on a small series of patients.

A study (Keller LMM et al., 2013) examined the advantages of treating large breasts (i.e. D cup size) with a commercially available custom-fit bra. The primary endpoint was the rate of acute radiation dermatitis. For the purpose of this study, different energy including 6MV, 10 MV, and 18 MV, and different techniques such as IMRT and 3D-CRT were used. The results indicated a high rate of dermatitis with the bra compared with no bra. The rate of grade 2 versus grade 3 dermatitis for IMRT and 3D-CRT were 87% vs. 64% and 100%vs.86%, respectively.

A recent study of a breast cup device (Do cup) performed by Arenas et al. (Arenas et al., 2014) compared two CT studies that were carried out on 12 cancer patients with large or pendulous breasts. In the first CT study, patients were wearing the breast cups. In the second CT, no breast cups were used. The Do cup is made of 0.5+- 0.05 mm thick transparent plastic material and attached to cloth strap cup for the unused breast. All patients were treated by 6 MV photons and dynamic wedges. To optimize the dose distribution, a field in field treatment planning technique was used. The field in field technique is an open field with subfields to provide higher or lower doses where needed. The main disadvantage of the breast cup is the skin toxicity due to failure to eliminate the skin fold. The surface dose increased from 28.1% to 47.7 % because of bolus effect caused by cup material. As a result, all patients had erythema, and 10 patients had moist desquamation in inframammary fold area

1.7 The aim of this thesis

This thesis investigates the underlying principles of physics relating to skin dose in radiation treatment for breast cancer. The primary goal of this work is to determine suitable design parameters for construction of a breast positioning device that will decrease skin reactions by eliminating skin folds for breast cancer patients undergoing radiation therapy. A suitably designed device may also provide the potential to reduce heart and lung dose in breast radiotherapy. Using a systematic approach to assessment of skin dose, breast positioning and state of the art materials, the overall aim of this work is to lay the groundwork to improve upon the results from the previous breast positioning devices described above.

Chapter two describes how a modern linear accelerator is used to deliver radiation therapy for breast cancer. The impact of MV x-ray energy on skin dose, as a function of breast size is demonstrated, as well as the impact of field size and beam incident angle.

In chapter three a treatment planning study was performed to assess the impact on skin dose of an in-house foam wedge breast positioning device currently in use at the BC Cancer Agency. Specifically, we performed a dosimetric analysis on cases previously treated with foam wedge and compared these results to plans performed on the contralateral breast without the wedge as well as with a simulated idealized breast positioning device.

Chapter four presents an experimental study performed to investigate the feasibility of using EBT3 GafChromic™ film (Ashland, NJ) to measure skin dose in the presence of a wedge shaped device to reduce skin folds. Radiation was delivered to phantoms on the

radiotherapy equipment at the Vancouver Centre. Results were compared with the treatment planning study in chapter three.

Chapter five investigates the radiological properties of two materials that are potential candidates for constructing a breast positioning device. A low density (Dow Styrofoam SM Insulation, Convoy Supply, and www.convoy-supply.com), high strength material (Prepreg 3K, Fibre Glast Developments Corp, and www.fibreglast.com) was compared to water and the commercially available foam product used for the in-house wedges studies in chapters 3 and 4.

In chapter six, conclusions are drawn and recommendations are made for future work.

Figure 1.1: The Schematic diagram of human skin showing: epidermis, dermis, and underling fat layer with average thicknesses of the epidermis and dermis.

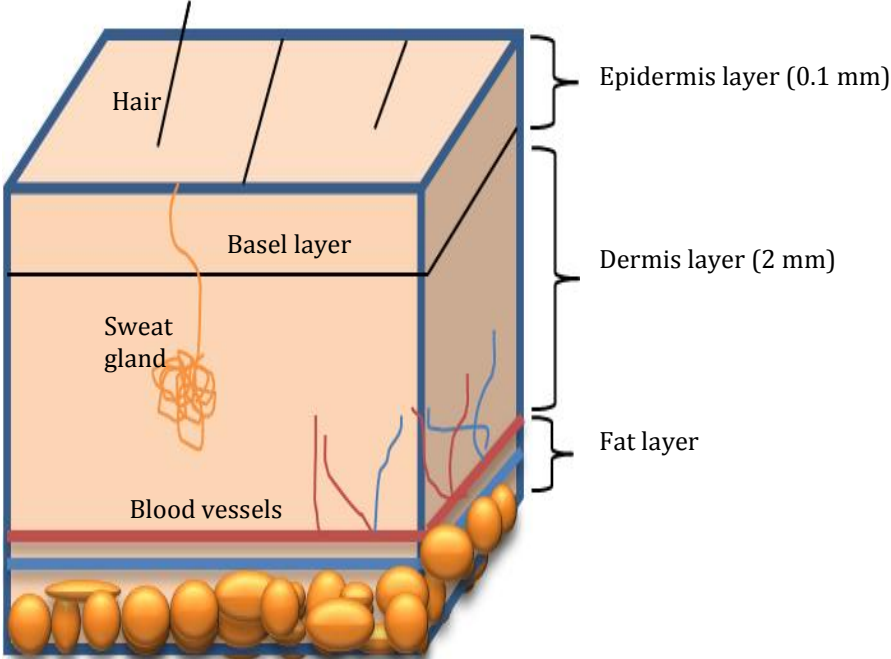


Figure 1.2: The graph shows decreasing kerma in red line and absorbed dose in black for a mega voltage x-ray beam incident on the surface from the left of the diagram.

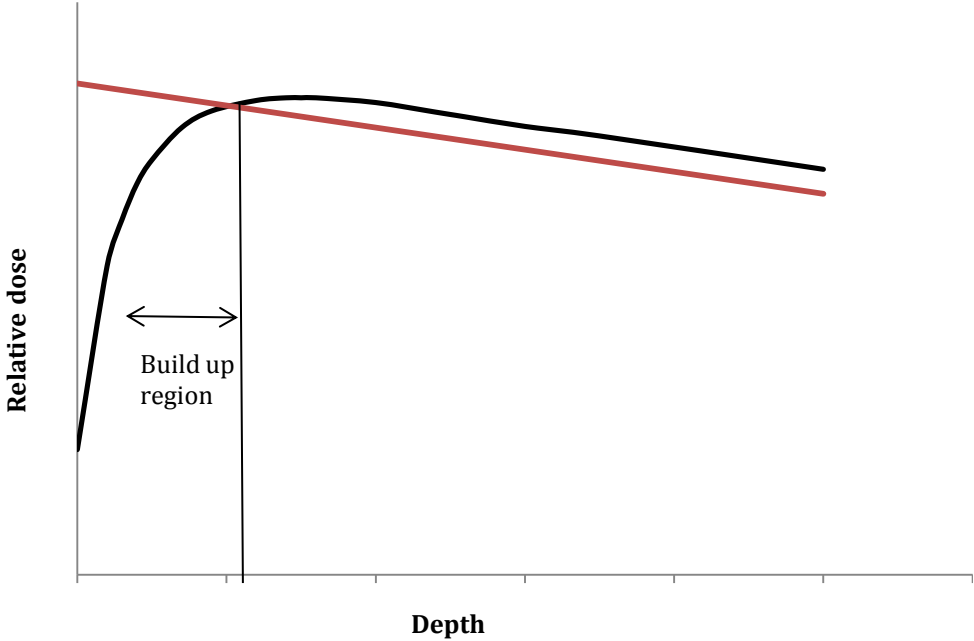


Figure1.3: Illustration of an example of patient positioned supine in breast board with both arms up.



Table 1.1: Breast immobilization literatures review.

Study	Study population	Device description	Dose measurement method	Surface doses	Toxicity	energy
<i>Cross, Elson, & Aron, 1989</i>	4 patients with cup size EE	a styrofoam cut out and an alpha cradle	Not applicable	Surface dose rose from 40% to 80%.	moist desquamation in the infra-mammary fold	4 MV in lateral decubitus position
<i>Bentel & Marks, 1994</i>	12 patients with large/flaccid breasts.	A reinforced polyvinylchloride (PVC) tube with Tape.	Not applicable	Not applicable	Patients developed a small area of moist desquamation.	6 MV. 3D-CRT.
Zierhut et al., 1994	7 large pendulous breast cancer patients	An Orfit immobilization: cast thermoplastic device	TLD	Increase the surface dose on patient from 47% to 64% and on phantom from 51% to 64%	86% of the studied cases developed erythema, and 14% had moist desquamation.	6 MV. 3D-CRT.
<i>Bentel, Marks, Whiddon, & Prosnitz, 1999)</i>	56 patients with large breast	Ring formed by PVC tube and support with a Velcro strap	Photon diode with scanning system	85% of maximum dose using the breast ring c/w 35% without.	60.7% of patients developed moist desquamation; and the other had erythema, and hyperthermia.	6 MV. 3D-CRT.
<i>Latimer, 2005</i>	Eight patients with large pendulous breast	Polyacrylic microshell shaped into a horse-shoe	-Parallel plate ionization chamber: Solid water and phantom - in vivo TLD	86% using the micoshell c/w 79% without.	Reduction in the severity of skin reactions.	Not applicable
<i>Keller LMM et al., 2013</i>	12 left side D cup	Thin fabric material, with thin plastic Bra an alpha-cradle cast on a 10-20% angled breast board.	Not applicable	Not applicable	(IMRT): Grade 2/3 skin toxicity 87% c/w 64% without (3DCRT) Grade 2/3 skin toxicity 86% c/w 100% without	6, 10, or 18 MV. IMRT & 3D-CRT
<i>Arenas et al., 2014</i>	12 patients, D cup	Breast cup, 0.50 ± 0.05 mm transparent plastic material	Film: Solid water and thorax phantom with silicone breasts	47.7% using the breast cups c/w 28.1% without.	All patients had erythema. Ten of the patients had moist desquamation.	6 MV. Field in field technique.

Chapter 2: Surface dose in megavoltage x-ray beams

2.1 Introduction

Megavoltage x-ray beams can offer skin sparing in breast radiotherapy, however tangential incidence of the beams as well as the irregular shape of the breast impact the magnitude of the skin sparing effect. This chapter will begin by providing a brief introduction to external beam radiotherapy with an emphasis on the concepts most important for breast treatments. Subsequently, this chapter will describe the skin dose as a function of treatment parameters. These will include the separation, field size, beam angle and beam energies.

2.1.1 Linear accelerator

Since the 1950s, the linear accelerator (linac) has become the primary modality for delivery of external beam radiation therapy. Linacs operate by using electric and magnetic fields to form a stream of fast moving electrons which are bent toward a tungsten target upstream of the patient to produce a beam of photon radiation. Linac-based external beam radiotherapy (EBRT) involves the use of these high-energy x-rays (megavoltage) to treat deep seated tumors.

Figure 2.1 shows a schematic diagram of the linac components. The linac has two main compartments; the stand and gantry. The stand holds the gantry, and is fixed to the floor. The gantry is attached to the stand and has the ability to rotate ± 180 degree around the patient. The primary Linac components that control the production of x-ray beams include a klystron or a magnetron, an electron gun, and an accelerating waveguide. The

electron gun injects the electrons into the waveguide tube synchronously with the injection of radio frequency wave pulses that are generated by the magnetron or klystron. By using these high-frequency waves, the electrons can be accelerated to high energies along the wave guide tube. Then, accelerated electrons are directed by magnet fields toward a tungsten target to generate bremsstrahlung x-ray photons (Khan, 2003, p 42-51).

Before the photon beam can emerge from the linac, it goes through a flattening filter, steering and monitor components (ionization chamber), and other collimation and shaping components such as the primary collimator, secondary collimator (upper and lower jaw), and multi-leaf collimators (MLCs). Using these components a linac can be used to treat all body sites by shaping and conforming x-rays beam to the tumor.

Treatment plans specify beam orientations, beam intensities and field shapes which are optimized to meet prescribed dose constraints. An approved plan that is developed in a treatment planning system can be transferred electronically to the linac for delivery.

2.1.2 Eclipse™ treatment planning system

Eclipse™ (Varian Medical Systems, Palo Alto CA), is a treatment planning system which is used to create and modify treatment plans. A treatment planning system (TPS) requires machine characteristic information such as isodose distributions based on the input of measured beam data as well as patient specific information such as CT images, tumor contours and dose prescriptions. Using a TPS, one can calculate, modify, and display patient specific dose distributions quickly and accurately, applying appropriate beam energy, field size and number, gantry angle, beam weighting, and intensity modulation. Two algorithms exist in the Eclipse treatment planning system for dose calculation: the

AAA, an anisotropic analytical algorithm and the PBC- pencil beam convolution algorithm (Neal, 1995; Chen et al., 2015). All calculations in this study were performed using the analytical anisotropic algorithm (AAA) version 11.0.31.

The PBC approach requires CT numbers of the patient's anatomy, as well as the value of dose kernel at the point of beam entry in the patient. To determine the dose at any specific point, a summation over the contributions of all pencil beams to that point is performed. In contrast, AAA is defined as a superposition of the pencil beam convolution algorithm (PBC) and deals with 3D contour shape and photon and electron interaction properties. Also, AAA does take into account the effect of the lateral charged particle equilibrium and inhomogeneous media, and this higher degree of precision in dose modelling is particularly important in regions of electronic dis-equilibrium such as the surface region. Therefore, AAA can be expected to show improved dose accuracy compared with the PBC method for skin dose calculations (Panettieri, Barsoum, Westermarck, Brualla, & Lax, 2009; Mayles, Nahum, Rosenwald, & Papanikolaou, 2007, p 574-578).

2.1.3 Factors impacting surface dose

2.1.3.1 Energy

Photon energy is one of the most important parameters impacting surface dose. It was mentioned earlier in chapter one (section 1.4.2) that the surface dose decreases with increasing beam energy. This is because the average penetration depth of megavoltage photons increases with increasing energy and thus so does the depth at which energy is transferred to electrons. In addition, the scatter is more forward directed for higher energy

photons. As a result of increasing the beam energy, the skin sparing is increased as the depth of maximum dose increases, moving away from the surface as shown in figure 2.2.

2.1.3.2 Field size

The surface dose is highly affected by electron scatter from the accelerator structure and the air above the patient surface (head scatter), and by back- or side-scattered electrons coming from the interactions between the photon beam and the patient (Gerbi, Meigooni, & Khan, 1987). As the field size increases, the head scatter will be increased as well as the patient scatter. For small field sizes (less than 10 cm), the predominant influence on surface dose is the beam energy as described above. For field sizes greater than 10 cm, more electron contamination from the collimator and flattening filter comes through the larger beam aperture. Moreover, as the field size increases, the phantom scatter increases. Consequently, PDD curves move towards the surface as the field size increases.

2.1.3.3 Obliquity

The term oblique incidence refers to the case where the beam axis is not perpendicular to the patient's surface. The incident angle is the angle between the beam axis and the surface of (phantom or patient). Oblique incidence causes a pull and tilt in the isodose curves from their vertical positions as displayed in Figure 2.4. PDD curves are pulled toward the surface as shown in Figure 2.5 and the degree of tilt and pull depends on the incident angle. As a result, skin sparing is reduced by increasing the obliquity and the depth of maximum dose moves closer to the surface for angles of incidence closer to zero (Gerbi et al., 1987).

Moreover, scattered electrons from the phantom or patient, which contribute to the surface dose, are higher in oblique incident angle than the scattered electrons in perpendicular incident angle. This is because the additional scatter electrons which result from excess phantom tissue in the oblique incident (Mayles et al., 2007, p 526; Khan, 2003, p284).

2.1.3.4 Source to surface distance (SSD)

Electron scatter from the components in the head of the machine is less likely to reach the patient as the distance between the linac head and the patient increases. Consequently, the impact of head scatter on surface dose decreases as the SSD increases. (Mayles et al., 2007, p 561).

2.2 Surface dose calculations in the Eclipse™ treatment planning system

The Eclipse™ (Varian Medical Systems, Palo Alto CA) surface dose calculation was validated using a Marcus ionization chamber to measure dose in a solid water phantom. Figure 2.6 shows the agreement between reference BC Cancer Agency Marcus ionization chamber data from the commissioning process and Eclipse™ data in the build-up region for a 6MV photon beam from a Varian CLIX linear accelerator (Varian Medical Systems, Palo Alto CA). A dose calculation grid size of $0.25 \times 0.25 \times 0.25 \text{ cm}^3$ was used. The depth dose was extracted from Eclipse by taking the dose profile along the central beam axis. The resolution of the Marcus chamber in depth is 0.01cm, which is substantially better than the resolution of the calculation. Marcus chamber data was corrected for side wall scattering during the commissioning process. Despite the grid size limitation of the Eclipse™ calculation, the measured and calculated doses agree within 2.2% in high gradient build-up

region. These results indicate that Eclipse™ can provide some useful skin dose information and should be adequate for the purpose of the following demonstration.

2.2.1. Demonstration of entrance and exit skin dose for a simple geometric phantom

In order to understand the behavior of surface dose as a function of energy and tissue thickness, the surface dose for an idealized breast treatment was simulated on a simple water equivalent phantom for 6 MV and 10 MV photon beams using Eclipse. A cuboid phantom of 40x40 cm² cross sectional area was constructed with varying thickness (t) ranging from 5 cm to 30 cm. Parallel opposed fields were placed on the phantom perpendicular to the 40x40 cm² surface and dose was calculated with a fixed field size (F.S) of 20x10 cm² and source to isocenter distance (SAD) of 100 cm, as shown in figure 2.7. A region of interest (ROI) defining the skin was contoured as the first 0.3cm of the phantom's body contour by using contouring tools. A structure was created by defining a 0.3 cm inner margin on the body contour, and then cropping the new structure from the body contour, leaving the skin ROI. Entrance dose and exit dose for each beam was measured separately to demonstrate this impact of increasing tissue thickness and energy. All doses were normalized such that the total dose from both beams at the isocenter was 100%.

The percentage mean dose in the ROI was explored by looking at entrance and exit dose individually and then summed for phantom thicknesses' of 5 cm, 10 cm, 15 cm, 20 cm, 25 cm, and 30cm as shown in figure 2.8. It is observed that the mean dose in the skin ROI (green line) increases with the increase in tissue thickness, first slowly and then dramatically beyond a 25 cm separation. The contribution from the entrance dose (blue

line) increases gradually, while the contribution from the exit dose (red line) decreases gradually. The 6MV data as shown in figure 2.4(a), demonstrate that the skin ROI dose rises from 70% to about 93% as the separation increases. The 10 MV data shown in figure 2.4(b), demonstrates that the skin ROI dose increases from 66.4% to 78% as the phantom becomes thicker. The skin ROI dose was fairly constant until the separation reached 20cm and 25 cm for 6 MV and 10 MV, respectively. Also, the data show that to keep the ROI dose less than 80% when using 6 MV; the separation can be increased up to 25 cm of separation, while for 10 MV, separation can be increased up to 30 cm.

As a function of separation, the mean dose in the skin ROI changes primarily because of attenuation and scatter of the photon beam in the phantom. As the phantom thickness increases, the dose at the isocentre and the exit surface decrease relative to the entrance dose due to increasing beam attenuation. Thus, relative to the isocentre, dose, the entrance dose increases and the exit dose decreases. The volume of phantom producing scatter also changes as the phantom thickness changes, but this has a less dramatic effect on relative entrance and exit dose compared with beam attenuation. Beam attenuation is more significant for the 6 MV beam compared with the 10 MV beam and thus entrance dose is remains higher for the while exit dose remains lower for 6 MV versus 10 MV. For instance, at 30 cm separation, the exit dose is about 24% for 10 MV and 21 % for 6MV, and the entrance dose is about 53.7 % for 10MV and 71.8% for 6MV. The difference is 3% in exit dose verses 18.1 % in the skin ROI for10 MV.

This simple demonstration illustrates the interplay between beam energy and tissue thickness when assessing surface dose in a very simple parallel opposed beam situation. There are two significant limitations in applying these results to predicting skin dose in

breast radiotherapy. In breast radiotherapy, beam incidence is not generally perpendicular to the breast surface. Oblique beam incidence will increase surface dose, as described in section 2.3.1. Also, the skin ROI was 0.3 cm thick. The epidermal layer is on the order of 0.01 cm thick. The dose gradient at the entrance surface is very steep so averaging over 0.3 cm will result in overestimation of the epidermal dose. Acute reactions are generally a result of dose to the epidermis while long-term side effects may be related to dose to deeper layers of the skin.

2.3 Conclusion

Surface dose increases as the thickness of the irradiated tissue increases for a parallel opposed beam arrangement. With a flat phantom surface and perpendicular beam incidence, keeping skin dose under 80% is achievable for a parallel-opposed beam arrangement using either 6 MV or 10 MV beams. However, in a breast cancer patient, the breast surface is neither flat nor perpendicular to the incident beam. From the basic principles of megavoltage x-ray beams, it is expected that surface dose for actual patients will differ from the simple case demonstrated here. Skin dose for breast patients will be discussed and considered in next chapter. The Eclipse AAA algorithm can be expected to produce results within 5% of measurement using a $0.25 \times 0.25 \times 0.25 \text{ cm}^3$ dose calculation grid size.

Figure 2.1: A schematic diagram of linear accelerator components in photon beam mode. 1) Stand, 2) Gantry, 3) Power supply, 4) Pulse modulator, 5) Klystron or Magnetron, 6) Electron gun, 7) Wave guide, 8) accelerated electron, 9) Bending magnet, 10) X-ray target, 11) Primary collimator, 12) x-rays photon beam, 13) Flattening filter, 14) Ionization chamber, 15) Collimator jaw upper and lower, 16) MLC, 17) Patient.

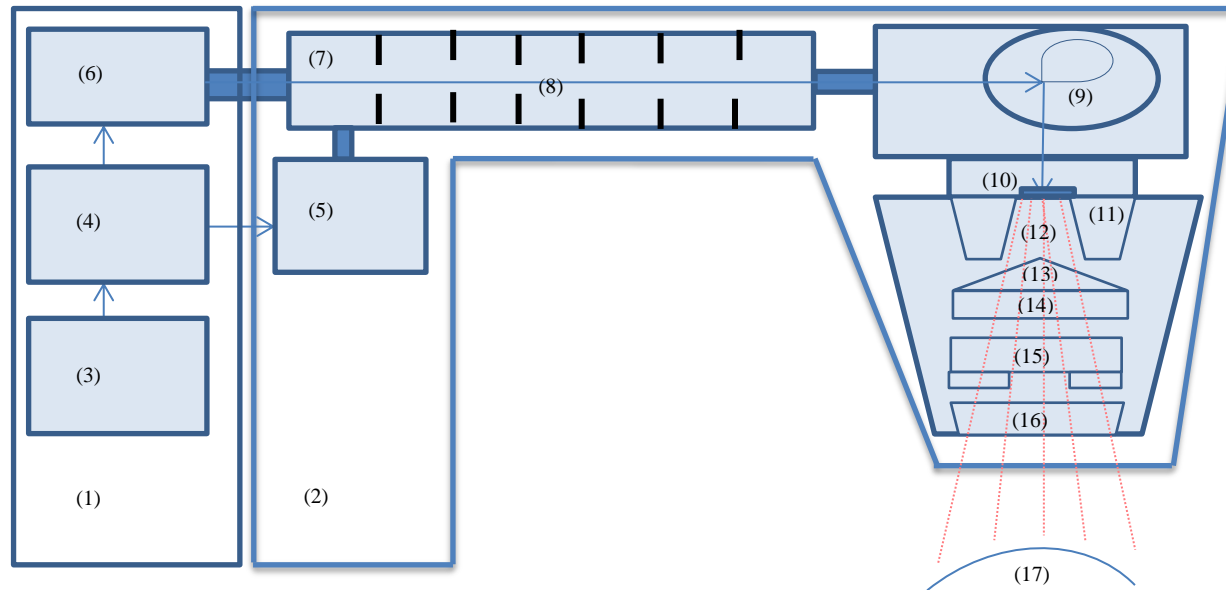


Figure 2.2: The Percentage depth dose curves of 6 MV (blue line) and 10 MV (red line) with 10×10 cm² field size, SAD= 100 cm, and normalized to maximum dose.

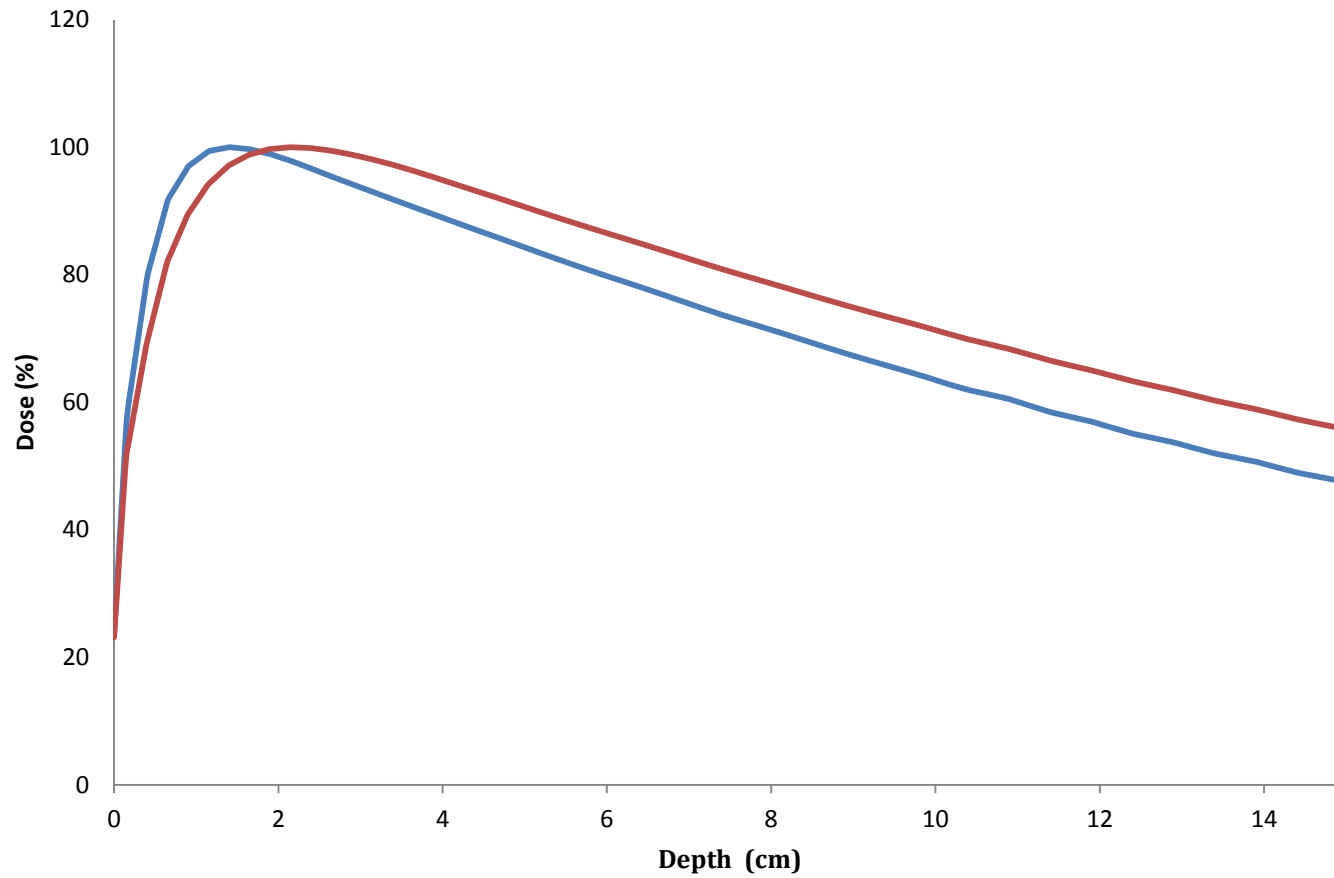


Figure 2.3: Percentage depth dose curves of 6 MV with 10×10 cm² field size (blue line) and 20×20 cm² (red line), and SSD =100 cm.

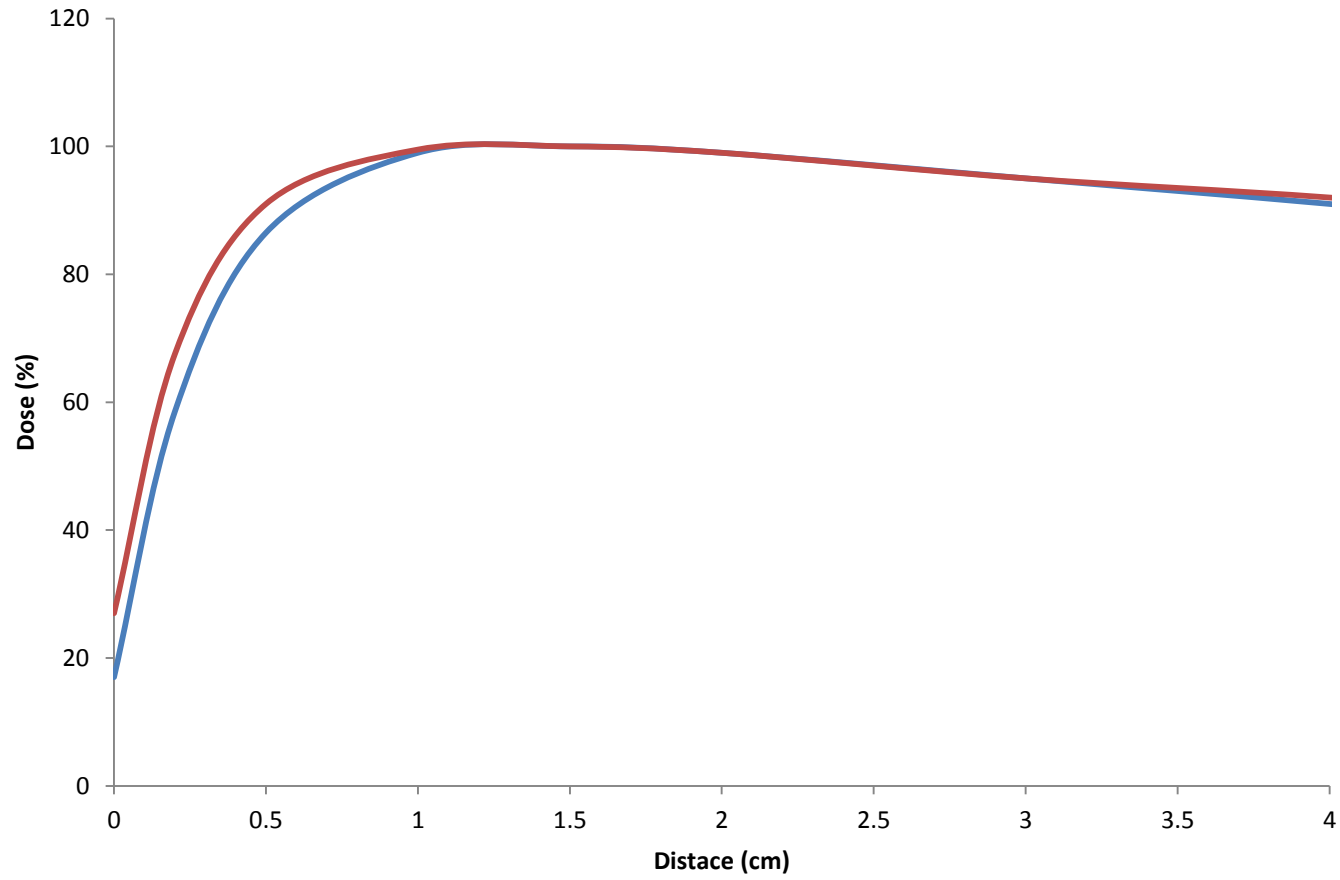
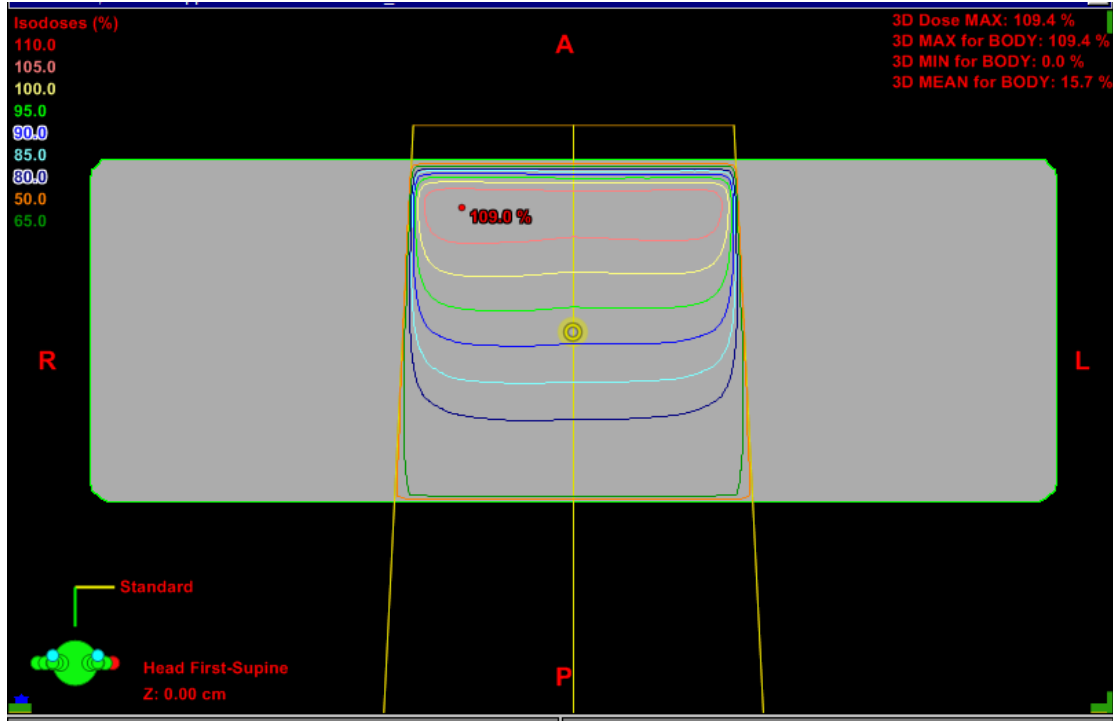


Figure 2.4: The dose distribution with different beam incident angle.

(a) Perpendicular beam incident angle.



(b) Tilted dose distribution of 30 degree beam incident.

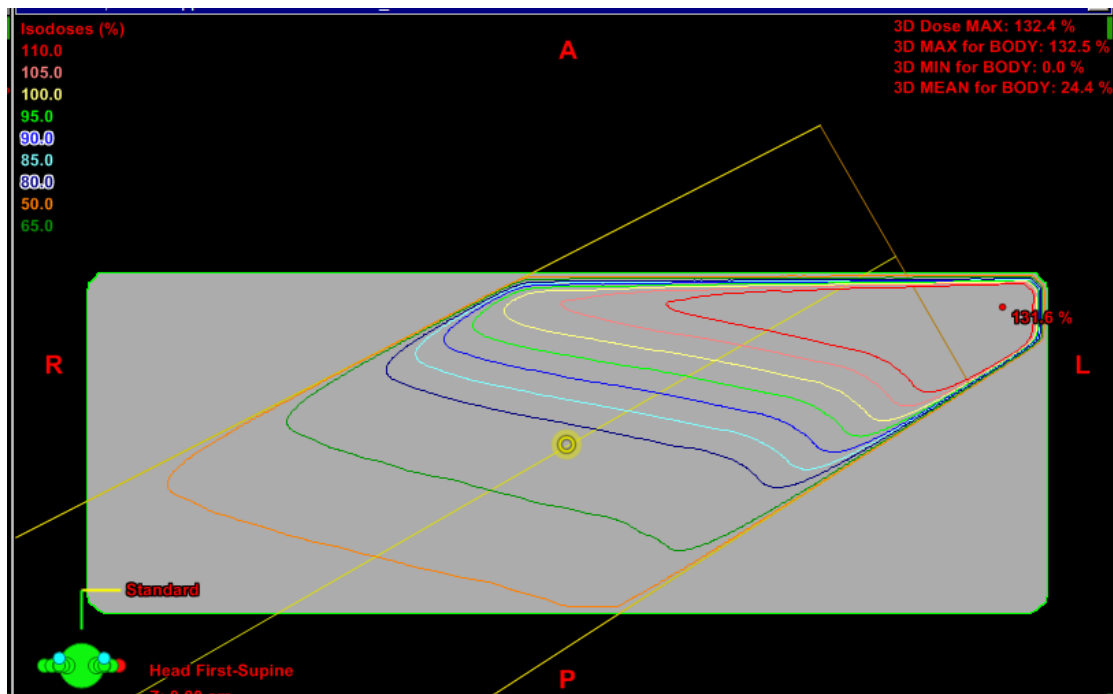


Figure 2.5: Illustration of the change in percentage depth dose as a function of incident angle 90 degree (blue line) and 30 degree (green line) for 6MV photon beam energy, 10×10 cm² field size, and a long vertical axis from figure 2.4.

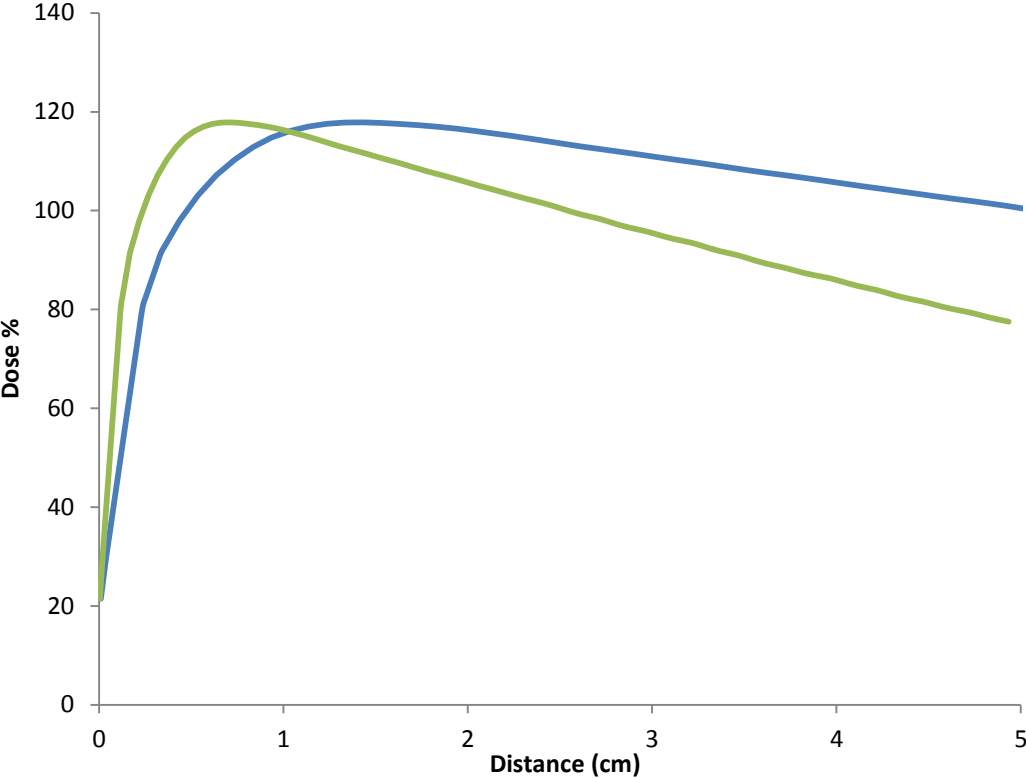


Figure 2.6: Validation curve for a fixed $10 \times 10 \text{ cm}^2$, which is obtained by using Marcus ionization chamber (green line) and Eclipse data (red dash line).

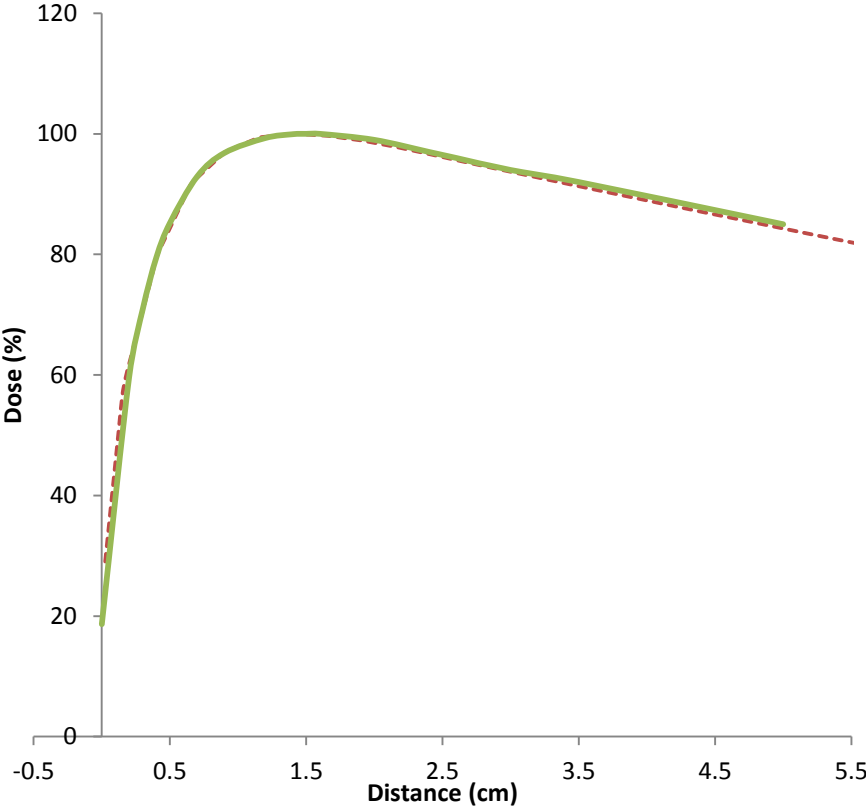


Figure 2.7: The Schematic of fields arrangement to determine the dose in region of interest (ROI) for cuboid phantom thickness (t) with fixing 100 cm SAD, 20×10 cm² field size (F.S) at the center, and parallel opposed beams.

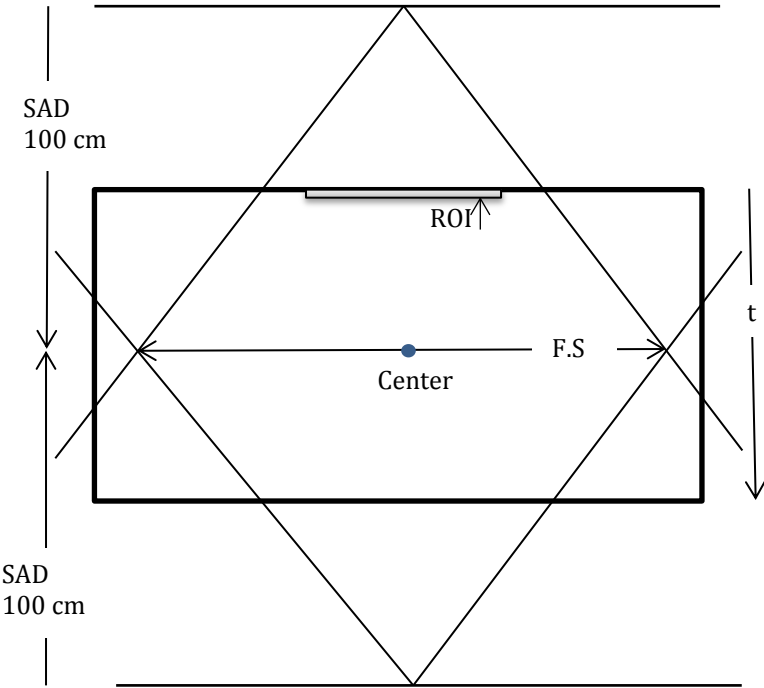
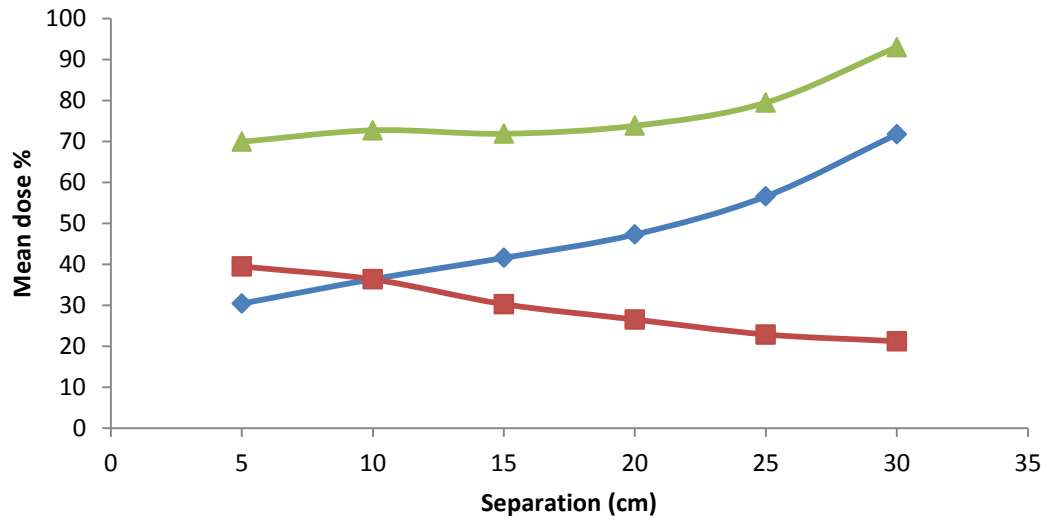
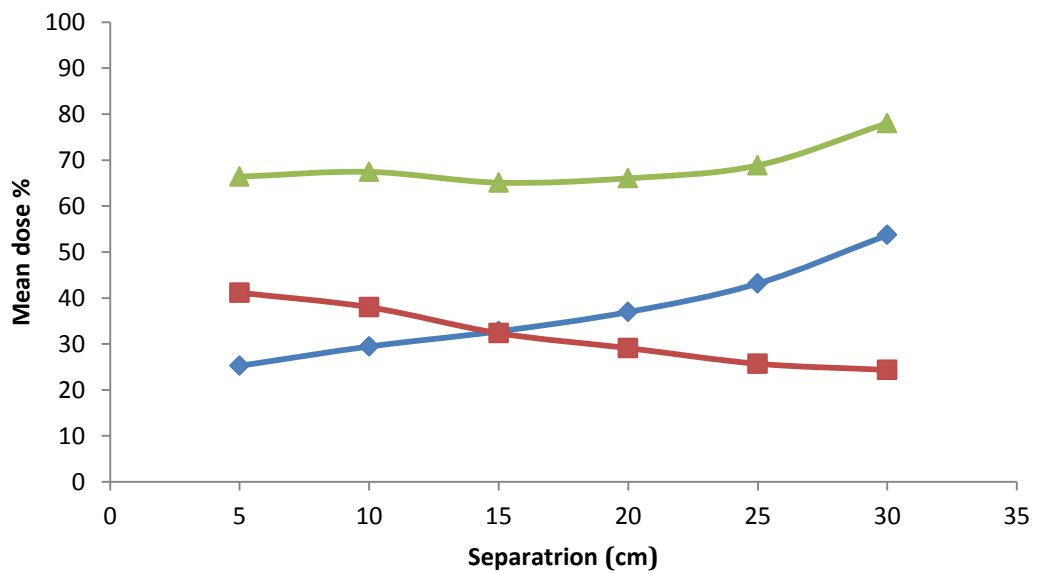


Figure 2.8: The mean dose of ROI (green line) is the combination of the entrance dose (blue line) and exit dose (red line) as a function of cuboid separation for:

(a) 6 MV x-ray.



(b) 10 MV x-ray.



Chapter3: Improving surface dose in skin folds during breast radiotherapy by modifying breast position

3.1 Introduction

There is a significant correlation between breast patient skin dose and skin toxicity in radiation therapy (Kelly et al., 2011). In spite of the sparing effect that comes from using modern treatment techniques, it is challenging to reduce skin dose in large or pendulous breasts undergoing radiotherapy, particularly in areas where there are skin folds. Examples of CT image data for breast radiotherapy cases with problematic skin folds are shown in figures 3.1 and 3.2. Breast tissue may fall inferiorly or laterally causing a skin fold where the breast comes in contact with the chest wall. This chapter describes a treatment planning study comparing skin dose associated with various breast positioning approaches designed to reduce skin folds in whole breast intensity-modulated radiotherapy (IMRT). Expected skin dose when using an in-house Styrofoam (Dow Styrofoam SM Insulation, Convoy Supply, and www.convoy-supply.com) wedge breast positioning accessory, currently in clinical use, is compared with skin dose using either no accessory or a hypothetical ideal breast positioning accessory.

3.2 Background

3.2.1 Contouring

In treatment planning for breast radiation therapy, reconstructed CT images are used to provide body and organ contours and the density of internal body structures. Target volumes and organs at risk are delineated on axial CT image planes. Target volume

contouring includes gross tumor volume (GTV), clinical target volume (CTV), and planning target volume (PTV). These contouring volumes are required in order to calculate and optimize the dose distribution with respect to the prescribed dose. Organs at risk (OARs), present normal tissue which, sensitive to radiation, may significantly impact treatment planning and/ or the prescribed dose (ICRU (International Commission on Radiation Units and Measurements), 1999). The OARs in breast cancer cases are primarily the heart and lungs. Moreover, there is no GTV in breast cases because the tumor is removed by surgical procedure. Therefore, the whole breast soft tissue is the CTV, and the PTV is defined by the posterior, superior and inferior tangent field borders, excluding a 0.5 cm rind of tissue inside the skin contour. The final PTV shape is almost a half-circle or oval in transversal (axial) view.

3.1.2 Tangent fields' set-up

The breast treatment is delivered by means of tangential fields. Two tangential fields are opposed, with a non-diverging posterior field edge (half beam block). To establish fields tangential to the breast, the gantry is rotated approximately 60 degrees from the vertical to produce the so-called medial beam and then an opposing beam with gantry rotation 180 degrees from the medial beam becomes the lateral treatment beam. The medial and lateral beams enter the body at about 30 degrees with respect to the breast surface. These fields enter the body on opposite sides of the breast along the same beam axis. The main advantages of opposed tangent fields are good target volume dose coverage, reduction in the dose to surrounding tissue, and avoidance of the contralateral breast. Moreover, half beam block fields (closing the field to half width) are used to avoid beam

divergence and decrease the involvement of adjacent organs such as heart and lung in treatment fields, minimizing the exposure of these organs. The actual field borders of the tangent fields are placed in the treatment planning system according to specification by the oncologist.

3.1.3 IMRT treatment planning technique

To optimize the target dose distribution, either forward or inverse planning techniques are available. It is essential to have a basic knowledge of the forward technique in order to understand the inverse planning technique. Conventionally, three dimensional conformal radiotherapy (3DCRT), a forward planning technique, is widely used for breast cancer treatment. A forward planning technique requires the planner to manually determine the contribution of each radiation field. Based on field borders which have been marked during simulation, the 3D- conformal plan will consist of two tangential and static fields with multileaf collimator (MLC) or blocks conforming to the PTV volume. MLC are composed of typically 80 or 120 tungsten leaves arranged in opposing pairs which create an irregular beam shape fitting to the target. The treatment planning system approximately models the MLC for dose calculations but in forward planning the operator specifies the MLC shape. Shielding of normal tissues, such as lung or heart, is achieved by adjusting the MLC (Barrett, Dobbs, Stephen, & Tom, 2009, P 21-23). Manually specifying beam weights and modifiers such as MLC and wedges in 3D conformal planning can be very time consuming and requires significant operator experience (Khan, 2010, p 468).

On the other hand, inverse planning makes use of an optimization algorithm to meet specified dose constraints for GTV, PTV, and OAR by modulating the beam intensity by

means of a moving MLC pattern. 3DCRT techniques have been replaced by IMRT in modern breast treatment planning. IMRT can deliver a more precise dose to the target area (Peart, 2015) because of sharp dose gradients (Van Gestel et al., 2013). In IMRT, a dynamic or moving MLC is used with either a fixed or moving gantry. There are two methods to deliver the IMRT using the MLC: step and shoot, and sliding window. The step and shoot technique uses static fields segments with the beam switched off between changes in the MLC position. The sliding window technique is characterized by MLC motion during beam delivery. (Barrett et al., 2009, p 23-24). In both cases, the target volume dose is delivered by combining multiple small beams or beamlets (Khan, 2010, p 481-483).

3.2 Materials and methods

3.2.1 Treatment planning

In this study, treatment plans from seven previously treated patients who had been assigned an in-house fabricated foam wedge as breast support during treatment were selected. These patients were treated by radiation therapy to the whole breast at the British Columbia Cancer Agency in Vancouver. 45 Gy in 25 fractions was prescribed to 2 patients, 42.5 Gy in 16 fractions was prescribed to 4 patients, and 50.40 Gy in 28 fractions was prescribed to one patient. The OARs (heart and lungs) were included in the IMRT optimization to reduce their dose to the standard clinical dose limits. These limits included an ipsilateral lung tolerance of $V_{20Gy} < 35\%$ (V_{20Gy} is the volume of lung receiving 20 Gy) and a heart tolerance of $V_{25Gy} < 5\%$ (where V_{25Gy} is the volume of heart receiving 25 Gy).

For treatment planning intent, CT scans were acquired with 0.25 cm slice thickness, with patients positioned in a supine position on a breast board with both arms up. Tangential fields were placed as described above. The PTV was contoured as follows: 1) the PTV coincided with the superior and inferior edges of the tangent fields and for optimization purposes, the PTV border was inside the superior and inferior field edges by 1.5cm. 2) The PTV was excluded from the heart, ipsilateral lung with a 0.5 cm margin, and from the skin by 0.5 cm margin 3) posteriorly the PTV was limited to no deeper than the anterior ribs. All contours are illustrated in figure 3.3.

For this study, each case was planned in three different ways to demonstrate the impact of the skin fold on skin dose. The skin fold is the area where the breast skin is in contact with the chest wall skin. The original plan used for treatment employed a small Styrofoam (Dow Styrofoam SM Insulation, Convoy Supply, and www.convoy-supply.com) wedge in an attempt to minimize the skin fold. This will be referred to as the wedge plan. To investigate the impact of the wedge, a second plan was optimized on the non-treated breast as there was no wedge used during the CT scan to position this breast. For the most part the treated and untreated breasts were fairly symmetric. This contralateral plan is referred to as the plan without wedge. A third plan was created on a modified breast contour that was designed to represent the hypothetical case where an ideal breast positioning device completely removes the skin fold. This is referred to as the modified breast plan. To create this plan, the breast contour was first modified to simulate the effect of pushing the soft breast tissue from the inferior or lateral region where a skinfold existed, either superiorly or medially to eliminate the fold, as shown in figure 3.4.

The skin dose for all three plans for each case was analyzed. To define the breast skin and skin fold for dose comparison purposes, a new structure was created by creating an inner margin (0.3 cm) on the body contour. The skin contour was obtained by cropping the new margin structure from the body contour. Figure 3.5 (a, and b) displays skin fold and body skin contouring. Also, a patient region of interest (PROI) was contoured in the same way as described in section 2.2, in order to compare skin dose on the beam entrance and exit surface as a function of breast separation. The breast separation was measured as follows: first, the mid-breast height was determined. Then, a line parallel to the posterior field boarder through the mid-breast height was drawn. The distance between the medial and lateral points where this line intercepted the skin contour was defined as the breast separation. This is different than the conventional breast separation often referred to in treatment planning practice defined as the separation between medial and lateral points on the skin contour at the posterior field border. The conventional definition was not well suited to the purpose of this study.

To produce valid dosimetric comparisons, the tangent field setup was kept the same for all three plans for each case. First in contralateral plans (without the foam wedge), the two tangential fields and MLC shape were taken from the plan with the foam wedge and only changing the gantry directions to target the opposite breast (left to right or vice versa). For the modified breast plans, the fields were changed in width and length in order to cover the modified whole breast to demonstrate the potential benefits of ideal breast position.

IMRT with sliding window technique was used in all plans with the exception of patients one and two, where a hybrid-inverse IMRT technique with sliding window was

employed. Hybrid IMRT consists of two tangent open fields and inverse optimized tangent fields. The IMRT plans which are the inverse optimized tangent fields accounted for 75% of the weighting and open tangent fields accounted for 25%. The open fields, as a base plan, were calculated with 10 MV photon beam and included shielding for the OARs by MLC leaves. After IMRT optimization was completed, the open fields were copied to the IMRT plan and then calculated altogether to produce a final plan.

The Analytical Anisotropic Algorithm (AAA) and 0.25 cm grid size were applied for dose calculation proposes in all plans. The treatment planning system with Eclipse version 10.0 was used to create IMRT plans using 6 MV x-rays or combined energies (6 and 10 MV) for the two tangent fields. In IMRT optimization, the constraints assigned for PTV coverage were 100% of the prescribed dose as a lower dose limit to 100% of the target volume and 105% of the prescribed dose as an upper dose limit to 0% volume, in order to attain the dose uniformity within the PTV. Similarly, for ipsilateral lung and heart, 20 Gy to 35 % volume and 25 Gy to 5% volume were set respectively as upper dose limits in the dose optimization to maintain the dose within the BC Cancer Agency and IMRT and VMAT constraints for breast radiation therapy.

3.2.2 Measurements

Breast skin dose in the PROI defined above was recorded for the five cases that used 6 MV photons only, in order to compare with the 6 MV data for the flat phantom case illustrated in Chapter 2. The following measurements were performed on all cases to determine the dosimetric differences between the three breast positioning methods.

1. PTV volume

2. Field length and width
3. Volume of 100% isodose for breast skin ($V_{100\%BS}$)
4. Skin fold volume
5. Skin fold 100% isodose volume ($V_{100\%SF}$)

3.3 Results and discussion:

The average dose for medial and lateral PROIs for the five cases using 6 MV x-rays is presented in Figure 3.6. The skin dose in these regions is between 50.4% and 60.8% of the prescribed dose. This PROI data as a function of increasing breast separation is consistently about 15% lower compared with the cuboid phantom results in section 2.2. This indicates that the IMRT approach is successful at producing distributed clinically acceptable dose on the surface of the breast, which is significantly less than the prescribed dose to the PTV. Lack of scatter due to the rounded breast shape compared with the flat phantom in chapter 2 results in lower surface dose, despite the oblique incidence of the tangent fields. This result is consistent with the clinical observation that acute skin reactions generally do not develop on the surface of the breast en-face to the beam.

The treatment parameters measured for all seven cases and the three positioning methods are shown in Figure 3.7(a-d). The blue columns represent the contralateral plans without a positioning aid; red columns represent the original plans with the wedge, and the green columns represent the modified breast plans.

No change in PTV volume was expected due to breast repositioning alone, however for plans done on the contralateral breast, some asymmetry in PTV volume was observed compared with the other breast. This is due to normal variation in left-right breast

symmetry and possibly to surgical intervention on the treated breast. The PTV volume did not change significantly for the modified breast plans in 4 out of 7 cases. In 3 cases the PTV for the modified breast was slightly smaller than in the original treatment plan. This is likely the result of a decrease in the volume of normal tissue situated inferior or lateral to the breast tissue which was included in the original PTV due to the non-ideal breast position. When modifying the breast contour to simulate ideal breast positioning, the volume of actual breast tissue was kept constant.

Field length, in general, is decreased as the PTV length decreased when using a breast positioning device. The modified breast plans consistently had the smallest PTV length for all seven cases, the field length is decreased when using the foam wedge compared with not using a wedge, except in one patient where the lengths with and without foam wedge are similar. A good demonstration of this effect can be seen in figure 3.1. Here, the breast on the left of the image was in its natural position, whereas on the right the breast is supported inferiorly by a foam wedge. It is clear that the field length required to cover the breast supported by the wedge is significantly less than that required to cover the unsupported breast. On the contrary, the field width is the highest in the modified breast plans for all cases, but shows less variation when comparing plans with and without the wedge. As shown in figure 3.4. The modified breast contours generally result in breast tissue sitting more anteriorly, requiring a wider field to provide coverage.

There is a consistent reduction in breast separation for the modified breast plans compared with the original plan for all patients. This is illustrated in figure 3.2 where it can be observed that the breast supported by a foam wedge, on the left of the figure, results in a much smaller breast separation compared with the unsupported breast on the right in the

figure. There is variation in relative separation across the seven cases likely due to unavoidable left –right breast asymmetry.

The breast skin dose volume data for the three different plans was compared in table 3.1. Notably, significant differences were found in the volume of skin receiving 100% of the prescribed dose ($V_{100\%BS}$). $V_{100\%BS}$ for the modified breast plans for all cases was $\leq 0.1 \text{ cm}^3$. $V_{100\%BS}$ without using any positioning device ranged from 2.7 cm^3 to 24.3 cm^3 , while $V_{100\%BS}$ using a foam wedge ranged from 1.5 cm^3 to 6.1 cm^3 .

To isolate the skin fold in this analysis, skin fold volume and skin fold $V_{100\%SF}$, are presented in table 3.2(a), and 3.2(b). It is demonstrated that using the foam wedge not only reduced the skin fold volume but also reduced the $V_{100\%SF}$ of the skin fold significantly. Skin fold $V_{100\%}$ without a wedge ranged from 8.3 cc to 15.4 cc. The reduction in $V_{100\%SF}$ resulting from use of a wedge ranged from 53.1% to 99.9%. Skin fold volume for the unsupported breast ranged from 10.8 cc to 18.0 cc. The reduction in the skin fold volume ranged from 5.22% to 97.49% when the breast was supported by a wedge. It should be pointed out that the Eclipse dose calculation is not expected to perform well on inner skin fold surfaces. Such surfaces exist when a foam wedge is placed in the skin fold, as shown on the right in figure 3.5 (a). Thus the $V_{100\%SF}$ values in Table 3.2 (a) should be validated by measurement and this will be the subject of the work in chapter 4. It should be noted that skin fold data for the modified breast plans is not presented here because the skin folds have been eliminated in these plans.

3.4 Conclusion

In breast IMRT, a fairly uniform skin dose of <65% of the PTV dose is achievable for en-face skin surfaces (i.e. not in a skin fold). When the breast falls inferiorly or laterally, the breast skin and chest wall skin will be in contact. As a result of this skin fold, the skin may receive a particularly high dose which is undesirable for breast radiotherapy as the first 0.15 cm of skin contains the most sensitive structures of the skin (Gerbi, Meigooni, & Khan, 1987). Using a simple foam wedge to position a pendulous breast off the chest wall can be helpful in reducing skin folds, reducing skin fold dose, reducing the breast separation and the field length required to cover the breast. However, by creating modified breast contours that simulate an ideal breast positioning scenario, it becomes apparent that there is significant room for improvement over the simple in-house foam wedge. Furthermore, the in-house foam wedge technique studied here is subject to significant variation in setup from day to day because the wedge is not fixed to any rigid structure, as it is inserted under the breast and held in place by the weight of the breast itself. Anecdotally, acute skin reactions are still observed in patients treated with the foam wedge. Thus, this study provides the motivation to design an improved breast positioning device and rigorously investigate the clinical impact of breast positioning in modern breast radiotherapy. The study of radiological properties of materials suitable for manufacture of such a device is the subject of Chapter 5.

Figure 3.1: The inferior skin fold and Styrofoam wedge effect in sagittal view. The yellow outlines represent the field's border; the mauve outline represents the Styrofoam wedge, and the PTV in red outlines. The difference in the inferior skin fold and the field length can be clearly seen between the right breast side (without wedge) and left breast side (with wedge).



Figure 3.2: The lateral skin fold in another patient. The yellow outlines represent the field's border, and the PTV in red outline. The difference in the lateral skin fold, field width and field separation can be clearly seen between the left breast side (without wedge) and right breast side (with wedge), and the reduction in field length.

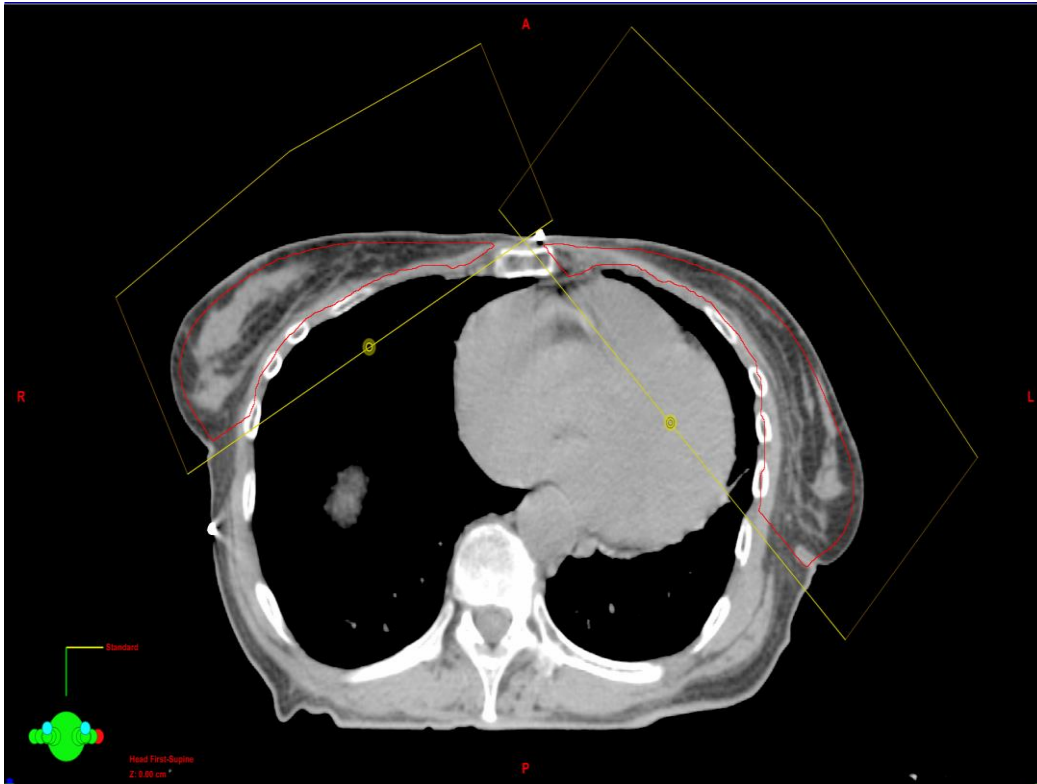


Figure 3.3: The PTVs and organ at risk contours on an axial CT slice images. The red outline represents the PTV, the orange region represents the heart, the cyan outline represents the left lung, yellow outline represents the right lung, and the green outline represents the body contour.

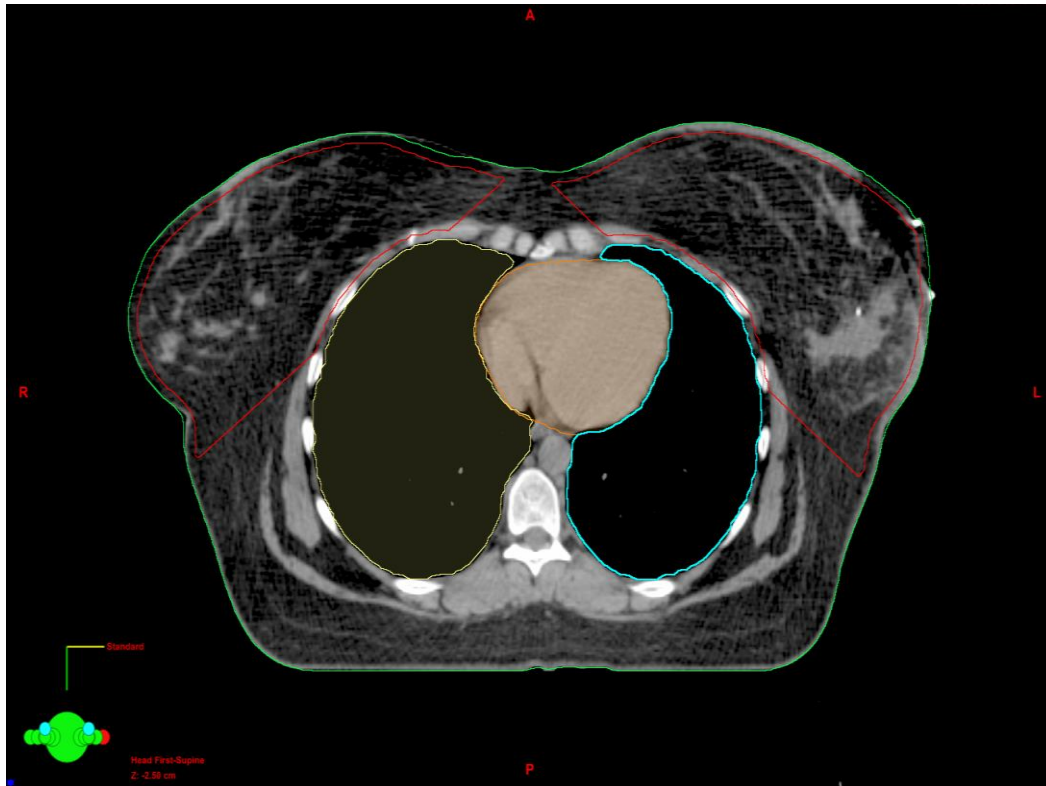


Figure 3.4: Breast re-positioning was simulated by contouring a modified breast on the axial CT image. The brown contour with gray filling represents the added strip above the original breast with zero HU CT value assignment, and dark blue strip represents the deleted part on this slice. It should be pointed out that the overall breast volume was preserved, although in the image it appears not to be the case.

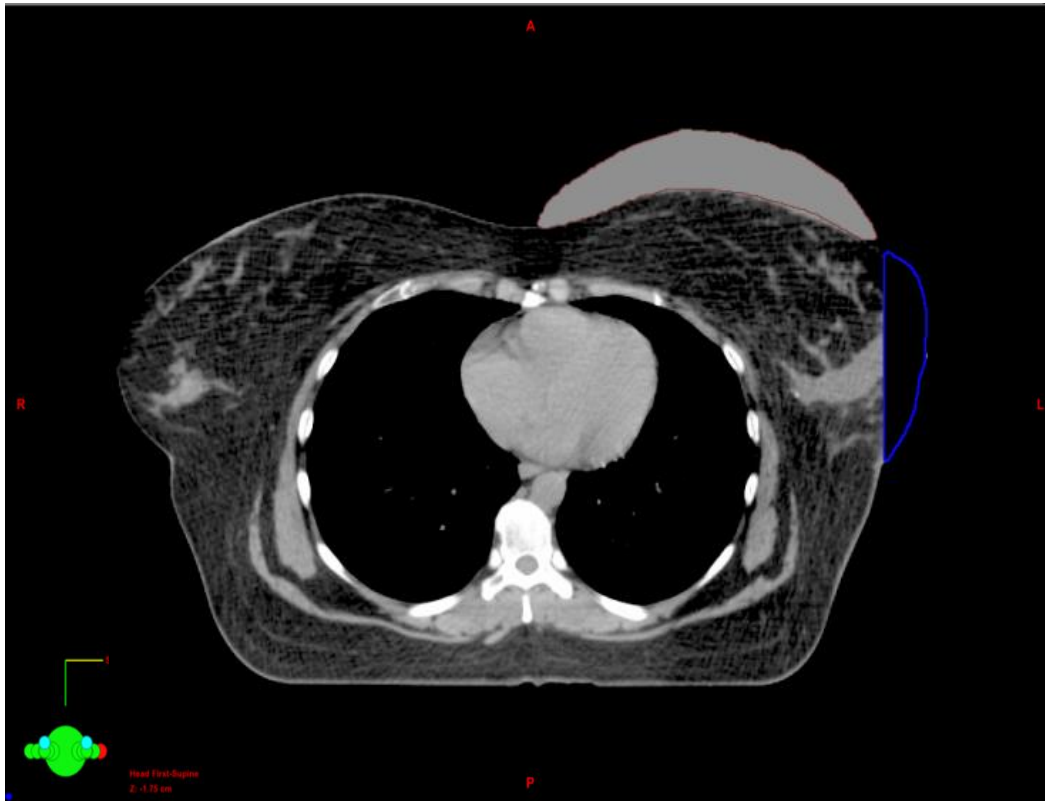
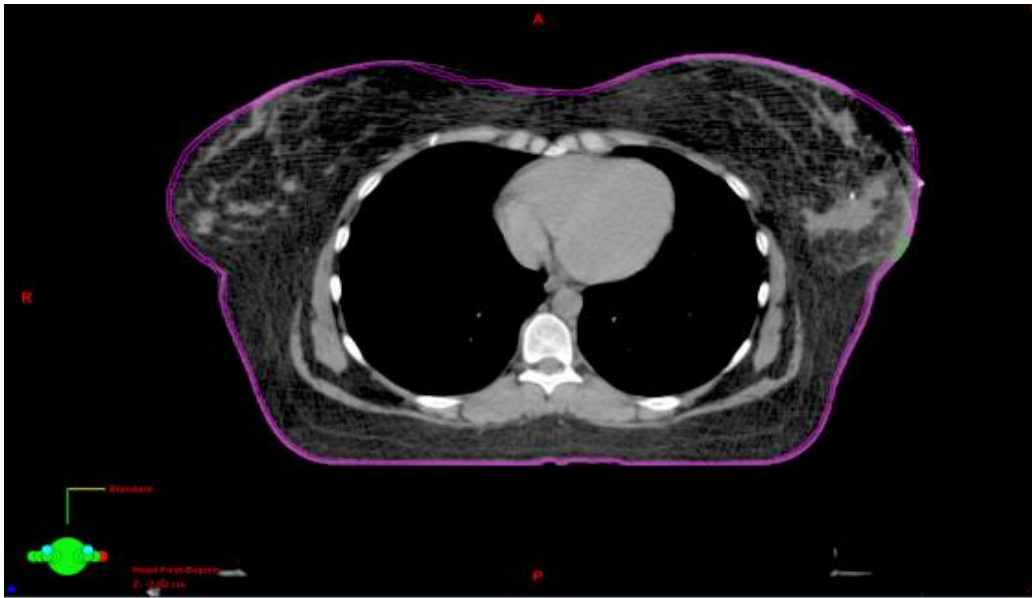


Figure 3.5: (a) 0.3 cm thickness of whole body skin contour in magnet color, and PROI in green color.



(b): Skin fold contour in pink color.



Figure 3.6: The mean dose of PROI (circles) as a function of patient breast separation for 6 MV x-rays, and phantom ROI (triangles) as described in chapter 2. The ROI is defined as 0.3 cm thickness from the skin of the patient and flat phantom.

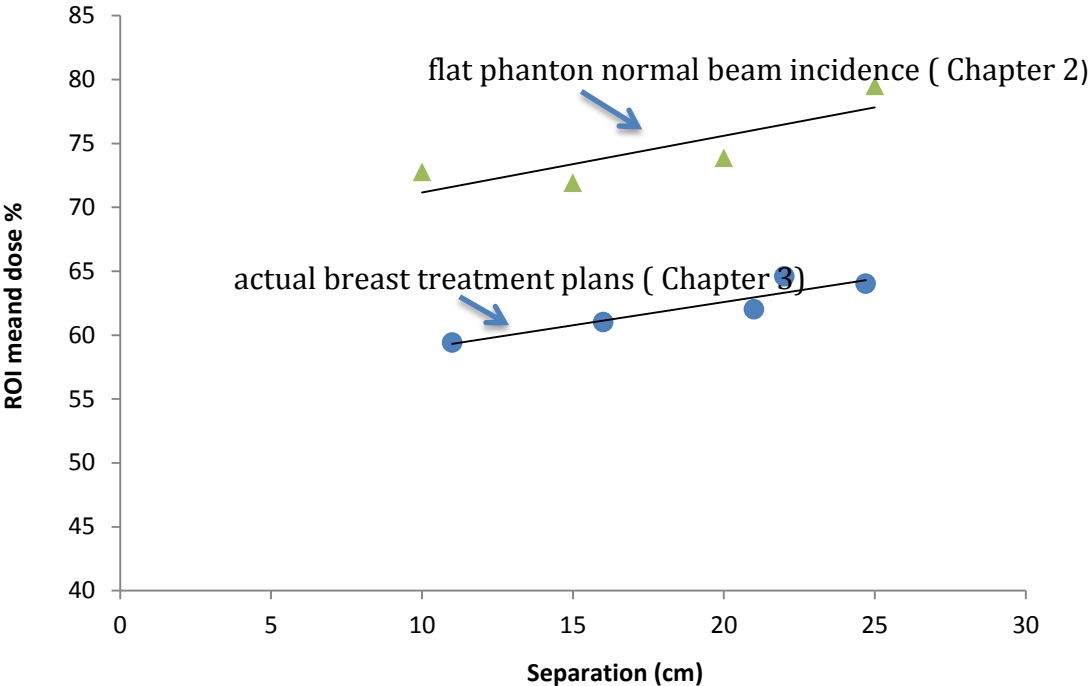
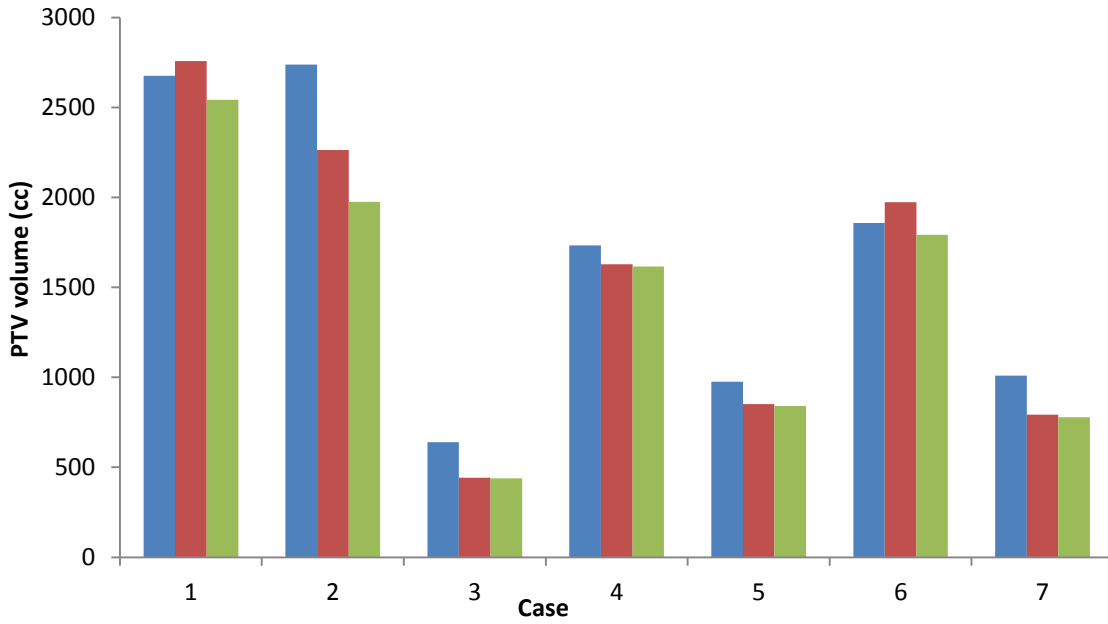


Figure 3.7 (a-d): Variation in treatment parameters generated by Styrofoam wedge (red columns), without Styrofoam wedge (blue columns), and modified breast (green columns).

(a) PTV volume.



(b) Field length

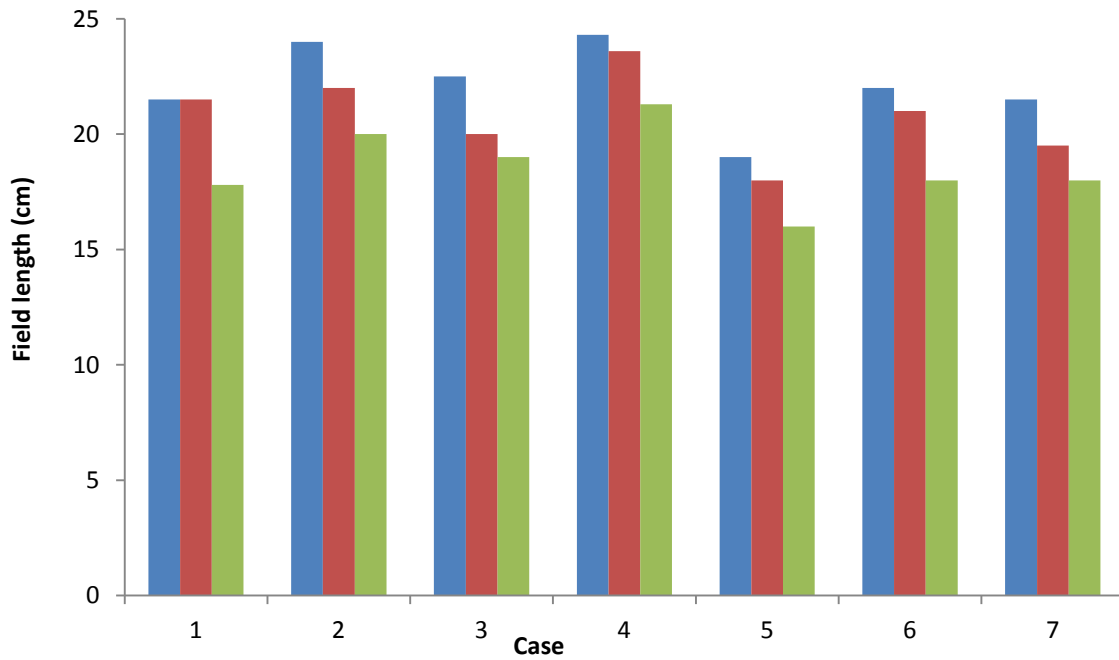
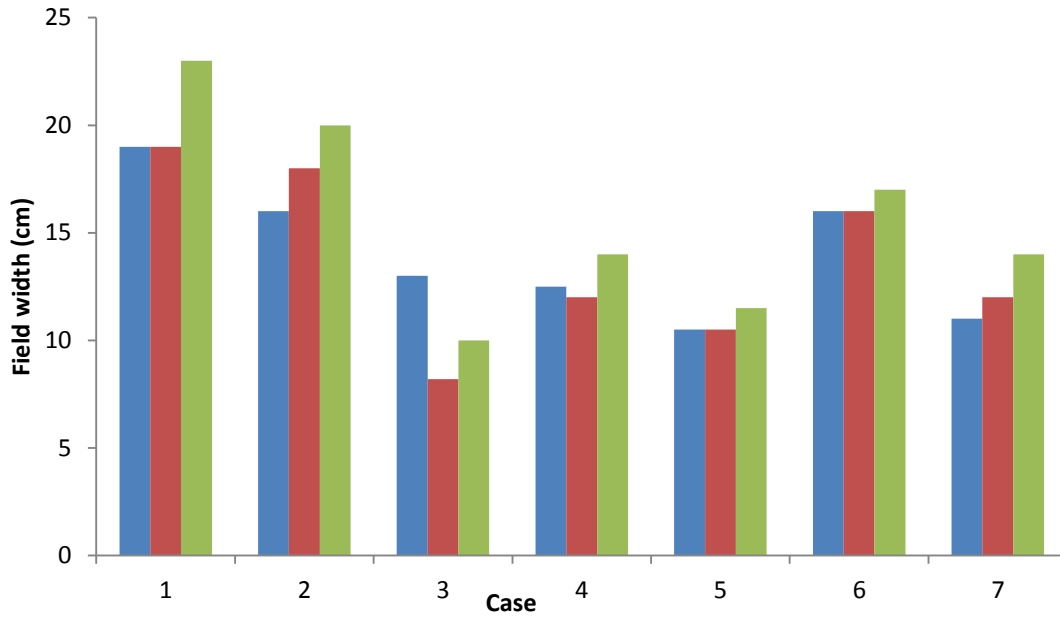


Figure 3.7 (a-d): Variation in treatment parameters generated by Styrofoam wedge (red columns), without Styrofoam wedge (blue columns), and modified breast (green columns).

(c) Field width.



(d) Breast separation.

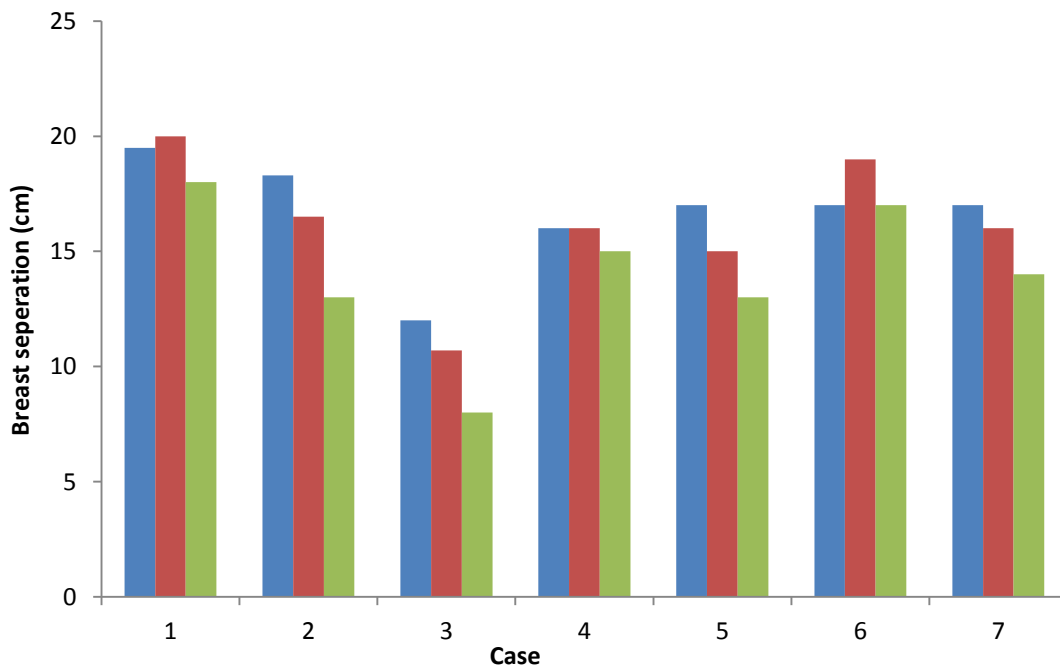


Table 3.1: The comparison of absolute volume in cm³ of 100 % dose of breast's skins (V100%_{BS}) calculated by the three plans: without wedge, with wedge, and modified breast plan.

Case	1	2	3	4	5	6	7
Without wedge plan	8.3	5.2	10.2	2.7	4.4	6.4	24.3
With wedge plan	3.8	1.5	0.1	1.5	0.9	2	6.1
Modified breast plan	0.1	0.09	0.03	0.3	0	0.003	0.008

Table 3.2: The comparison of with and without wedge plans of:

(a) Absolute volume (cm³) of 100 % dose of breast's skin fold (V100%_{SF}).

Case	1	2	3	4	5	6	7
Without wedge plan	8.3	4.6	11.5	3.2	3.5	4	15.4
With wedge plan	1.07	0.07	0.01	1.5	0.6	1.6	3.4
Reduction %	87.1%	98.5%	99.9%	53.1%	82.9%	60.0%	77.9%

(b) Skin fold volume.

Case	1	2	3	4	5	6	7
Without wedge plan	10.77	6.37	15.66	15.12	9.55	12.26	18.03
With wedge plan	6.14	0.16	1.55	8.43	1.47	11.62	5.51
Reduction %	43.0%	97.5%	90.1%	44.3%	84.6%	5.2%	69.4%

Chapter 4: Film dosimetry for breast surface dose

4.1 Introduction

The focus of the present chapter was to investigate an experimental technique for validating how a separation between the chest and breast skin surface, created using an in-house Styrofoam wedge, as discussed in chapter 3, affects surface dose. For this purpose, the EBT3 Gafchromic™ (Ashland, NJ) film dosimetry system was chosen to perform dose measurements in surface regions for IMRT breast treatment plans on an anthropomorphic phantom.

4.2 Method and materials

4.2.1 CT and treatment planning calculation

A rigid anthropomorphic phantom was prepared for breast treatment planning to simulate a patient. A patient's breast with 4 cm deep skin fold was mimicked using a rounded water bag attached to phantom's chest wall. To lift the breast and create separation in the skin fold region, a 45° Styrofoam (Dow Styrofoam SM Insulation, Convoy Supply, and www.convoy-supply.com) wedge was constructed and shaped from the low-density blue Styrofoam used clinically. The phantom was immobilized on a breast board in the supine position. Two CT images of this phantom were acquired at 0.25 cm slices thickness on the CT scanner, one with no Styrofoam wedge and other with the 45° Styrofoam wedge.

The CT images were exported to the treatment planning software (Eclipse), and the body contour was obtained using the Eclipse software. The PTV and OAR contours were

manually delineated and two IMRT plans were generated as described in the previous chapter.

4.2.2 Film calibration

Fourteen pieces of film were cut from a single EBT3 GafChromic™ film (Ashland, NJ) sheet. A dot mark was made in the top right of each film to indicate the orientation. Seven films (10×5 cm²) were used for calibration, and the remaining seven (three 6.5cm ×3 cm pieces and four 4.5×2 cm²pieces) were used to experimentally verify the planned dose. The phantom which was used to sandwich the calibration film pieces is composed of 40x40 cm² solid water phantom slabs of thickness ranging from 0.5 cm to 10 cm using an SAD set up, the field size at the isocenter, at 1.5 cm depth, was 10x10 cm². The film dosimeters were irradiated with gantry rotation of zero degrees. Therefore, the incident beam axis was perpendicular to the plane of the film. The calibration setup is shown in figure 4.1.

Each film dosimeter was irradiated individually with a 6 MV photon beam. A Varian CLIX linear accelerator (Varian Medical Systems, Palo Alto CA) was used to deliver between 50 cGy and 350 cGy. One piece of film was not exposed to radiation to provide for a 0 Gy reading. This set of the calibration films were irradiated and analyzed at the time of experimental dose verification on the breast phantom to avoid problems with time dependence of the film response.

4.2.3 Breast phantom dose delivery

An isocentric technique with SAD of 100 cm was used to set up the phantom on the treatment couch to match the CT simulator set up. An inferior inframammary skin fold approximately 4 cm deep was created under the water bag. A fixed mark was used to

reproducibly place the films and the wedges on the phantom. A Varian CLIX linear accelerator (Varian Medical Systems, Palo Alto CA) was used to deliver the two IMRT plans. In the first irradiation done without the Styrofoam wedge, three pieces of film were placed as shown in figure 4.2. The first film piece was placed between the breast and chest in the skin fold (a: without wedge). The second and third film pieces were on the right (b: lateral) and left (c: medial) sides of the breast. In the second irradiation, the wedge was inserted between the breast and chest wall in order to create separation. The fourth (a-upper: breast with the wedge) and fifth (a-lower: chest with the wedge) film detectors were accurately positioned on the upper and lower surfaces of the wedge with tape. The sixth (b: lateral with the wedge) and seventh (c: medial with the wedge) film pieces were placed at the same medial and lateral positions used above. The second irradiation film positions are shown in figure 4.3. An additional advantage of the dot mark was to indicate the inferior direction on the film.

4.2.4 Film analysis

All films were scanned at least 12 hours after irradiation using an Epson Expression 1000 XL flatbed scanner. As the scanner lamp warmed up, the light intensity could have been changing (Saur S. & Frengen, 2008). In order to avoid problems associated with that, several scans were performed without any films placed in the scanner prior to scanning the irradiated films. Also, to prevent fingerprints on the films which could lead to systematic error, the film was handled with a glove as it was placed on the scanner bed. All films were aligned and scanned in the same orientation using the existing QA Pro software and were stored as 16-bit, TIF images with a resolution of 72 dpi.

The TIF images were exported and analyzed using MATLAB software R2013a after the scanning process. All film data was separated into green, blue, and red channels. The red channel was chosen for analysis because the red channel was the most sensitive for the dose range of interest. The dose profiles were averaged along the longitudinal direction in all film measurements.

To validate the film readings, dose in the surface region from a fixed 10x10 cm² field were obtained using a solid water phantom and a Marcus ionization chamber and the results (Joel B.) compared to those from the EBT3 film. A calibration curve was created from the calibration films, as shown in figure 4.4, and was used to convert the film pixel values to dose.

4.3 Results and discussion:

The radiochromic film has the property of high spatial resolution and low spectral sensitivity and thereby makes it a suitable dosimeter for surface dosimetry (S. Saur, Fjellsboe, Lindmo, & Frengen, 2009). An agreement within 4% was found between ionization chamber data and EBT3 readings, which are shown in figure 4.5.

The digitized film images, as shown in figures 4.6 and 4.9, with their identifying position labels showed in figures 4.2 and 4.3., were converted to dose and normalized to the prescription dose of 265.6 cGy. The impact of the 45° Styrofoam (Dow Styrofoam SM Insulation, Convoy Supply, and www.convoy-supply.com) wedge can be seen on the digitized film images. The dose drops as we traverse the film from 0-6.5 cm, in the direction corresponding increasing wedge thickness, as seen in figure 4.6. Along the surface of the breast in contact with the wedge, there is little impact on the skin dose compared with the

case without the Styrofoam wedge. However, the surface dose along the chest with the foam wedge in place shows a more dramatic reduction.

Figure 4.7 illustrates the dose profiles measured from the films shown in figure 4.6 with and without the Styrofoam wedge. The blue line shows the dose profile without the wedge in place where the breast is in contact with the chest and the film is in the skin fold. The red line and green line show the dose on the breast surface and chest surface respectively, with the wedge in the skin fold, separating these two surfaces. The film measurements show a degree of noise in the data which is approximately 1%. All three dose profiles agree to within 5% near the thin edge of the wedge (0 cm position). With the foam wedge in place, the chest dose profile drops faster than in the non-wedged set up with increasing distance from the thin edge of the wedge. This would be expected due to less scatter to the chest surface from the overlying breast. The dose profile for the breast surface with the wedge in place is very similar to the dose profile without the wedge, with a slight increase in dose with the wedge in place at 5 cm from the thin edge of the wedge. Since the majority of scattered dose to this breast surface comes from the overlying breast itself, this result could be expected. The slight increase in dose is likely a result of the change in shape of the water bag (breast) with the wedge in place which is evident in figure 4.8.

Figures 4.10 (a) and (b) show the comparison of dose profiles for the medial and lateral surfaces of the breast shown in figure 4.9 with and without the Styrofoam wedge. The level of noise shown in these film measurements corresponds to less than 1%. The results indicate that the lateral surface dose is higher than the medial side in both plans. Without the Styrofoam wedge, the lateral dose (entrance beam angle 123°) ranges from

58.3% to 61.1%, and the medial dose (entrance beam angle 57°) ranges from 47.5% to 48.7%. Using the Styrofoam wedge slightly decreases the surface dose laterally (up to 2%) while slightly increases the surface dose medially (by 3%), possibly as a result of increased medial- lateral breast symmetry with the wedge in place or film positioning

These results show good agreement with the results of the treatment planning study in chapter 3 and the flat phantom data from chapter 2 which are reproduced in Figure 4.11 for the convenience of the reader. The breast phantom used here in chapter 4 has a breast separation of 18.5 cm. Mean skin dose for breast treatment plans was between 50% and 60% of the prescribed dose in a 0.3 cm thick skin PROI. The effective thickness of the film is less than 0.1 cm (Gafchromic EBT3 film thickness) thus the film data should be systematically lower than the Eclipse PROI data. Points dose measurements in Eclipse at points indicated on figure 4.12 are tabulated in Table 4.1 and indicated on Figure 4.9 for comparison with the film data. A comparison between calculated and measured point doses exhibits a varying level of agreement. This is possibly because the position of the points used in the dose calculations was slightly different than the position on the film in the measurements.

4.5 Conclusion

This study investigated the feasibility of measuring skin dose with EBT3 GafChromic™ film (Ashland, NJ) in breast skin folds to assess the impact of a simple Styrofoam wedge breast positioning device. The Styrofoam wedge creates a separation between breast and chest wall skin and this separation could allow for decreased scattered dose to the chest and breast surface and reduction in dose buildup to the skin. The EBT3

GafChromic™ film results reveal a decrease in surface dose along the chest as a consequence of the air gap with the wedge in place. Changes in water bag shape impact the breast skin dose distribution with the Styrofoam wedge in place. Dose to the breast skin surface is less impacted by the wedge than the chest surface dose is. Further separation of the breast from the chest might achieve further reduction in breast skin dose. Furthermore, these measurements illustrate the difficulty of measuring the surface dose in breast folds using a non-realistic breast due to a significant change in water bag shape with a wedge in place. The film technique has been shown to produce reliable measurements of skin dose on medial and lateral breast surfaces.

Figure 4.1: Photograph of the calibration set up with EBT3 film placed at 100 cm SAD with 1.5 cm solid water slab above the film and 15 cm solid water slab under the film. A 10×10 cm² field size and 6 MV x-ray photon beam were used to irradiate the film.

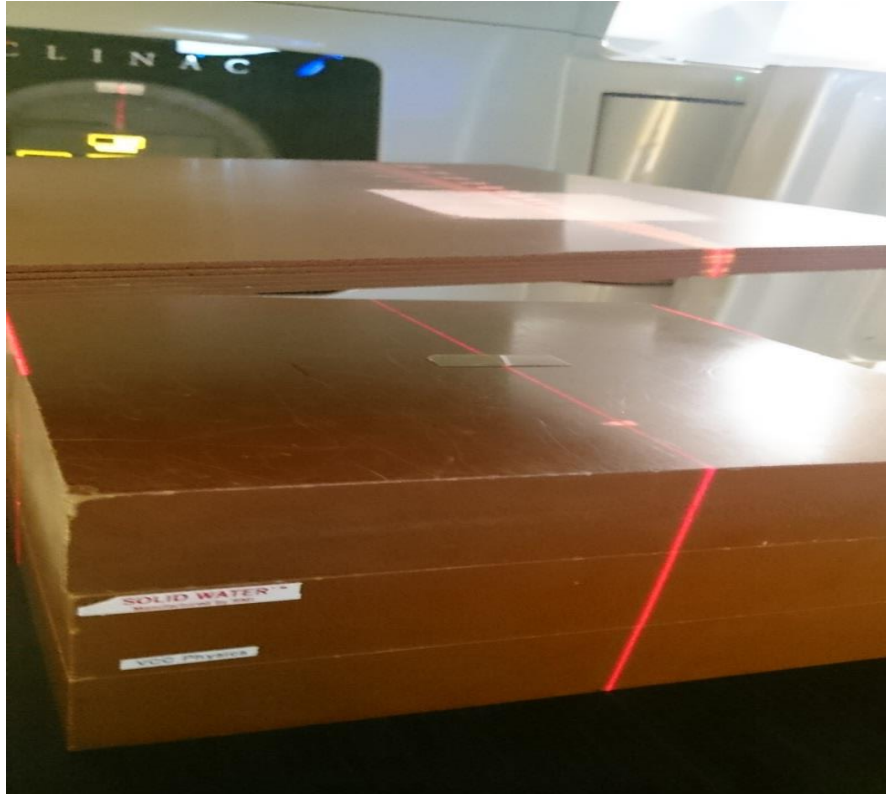


Figure 4.2: Photograph of the phantom set up for dose delivery without using foam wedge. EBT3 film locations, (a) first film placed between the breast and chest, (b) second film placed on the right (lateral) side of the phantom, , (c) third film placed on the left (medial) side of the phantom.



Figure 4.3: Photograph of the phantom set up for dose delivery using foam wedge. EBT3 film locations, (a-upper) fourth film placed under the breast above the foam wedge, (a-lower) the fifth film is also under the foam wedge on the chest surface (b), the sixth film is placed on the right (lateral) side of the phantom, (c) the seventh film is placed on the left (medial) side of the phantom.

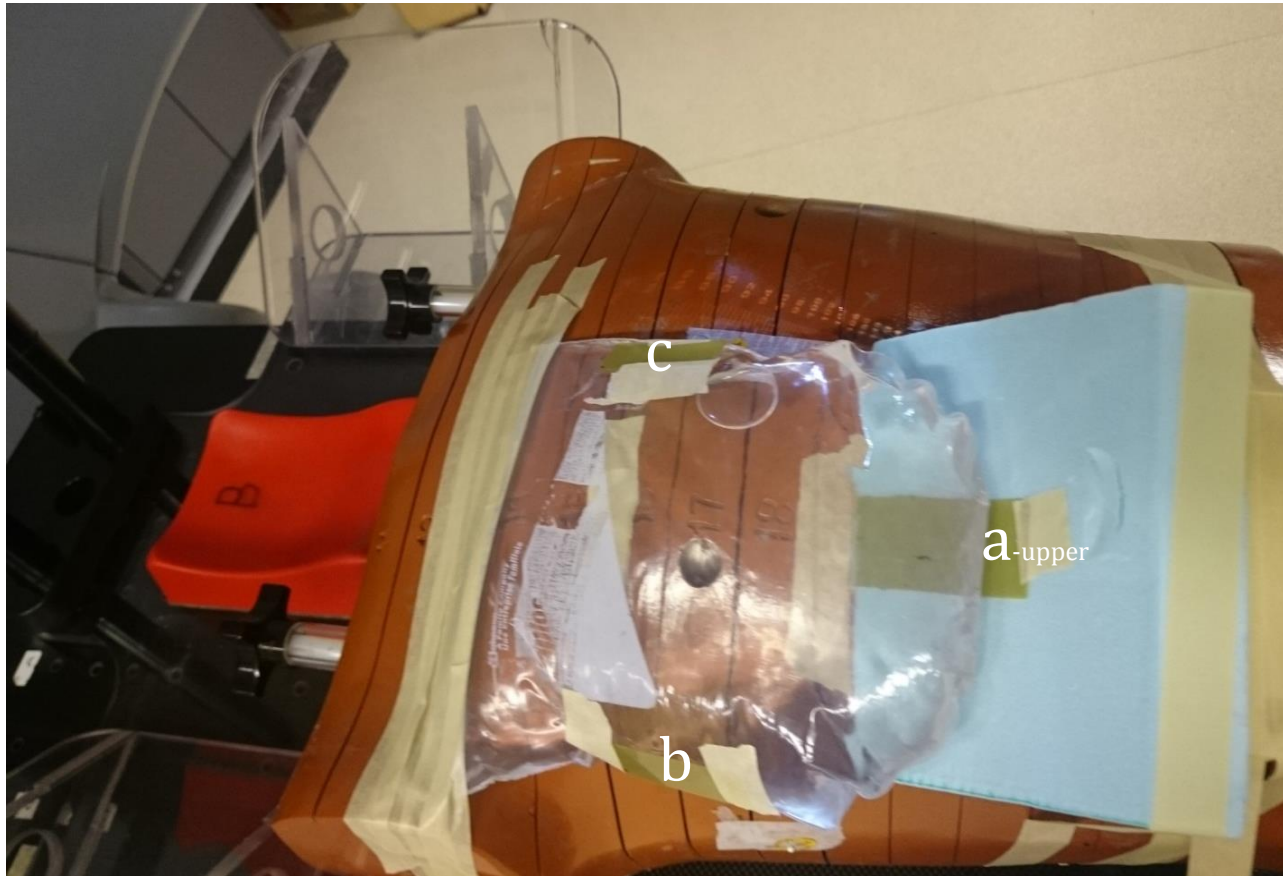


Figure 4.4: The film calibration curve in red channel for the flatbed scanner as determined in solid water phantom for 6 MV photon beam and 10×10 cm² field size.

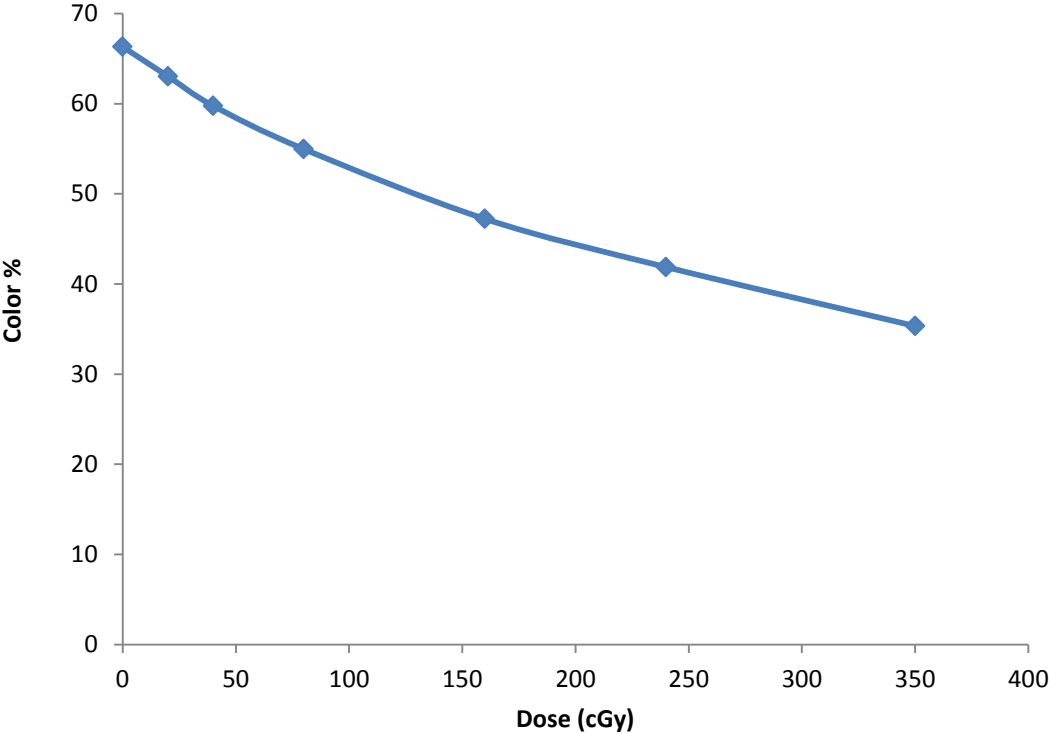


Figure 4.5: The validation curve for a fixed 10×10 cm² field size, 6 MV photon beam and the depth doses which obtained by using Marcus ionization chamber (blue line) and EBT3 films (red line).

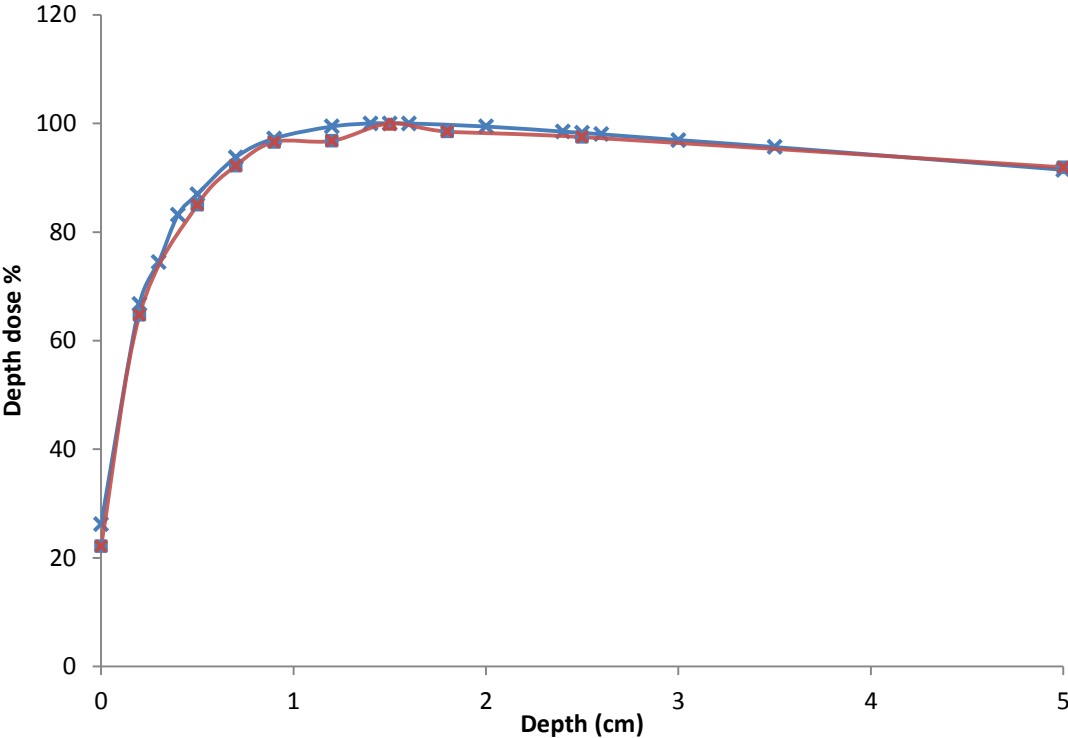


Figure 4.6: The surface dose measurements for (a: film in skin fold without foam wedge), (a-upper: breast film with wedge), and (a-lower: chest film with foam wedge) films as shown in figures 4.2 and 4.3.

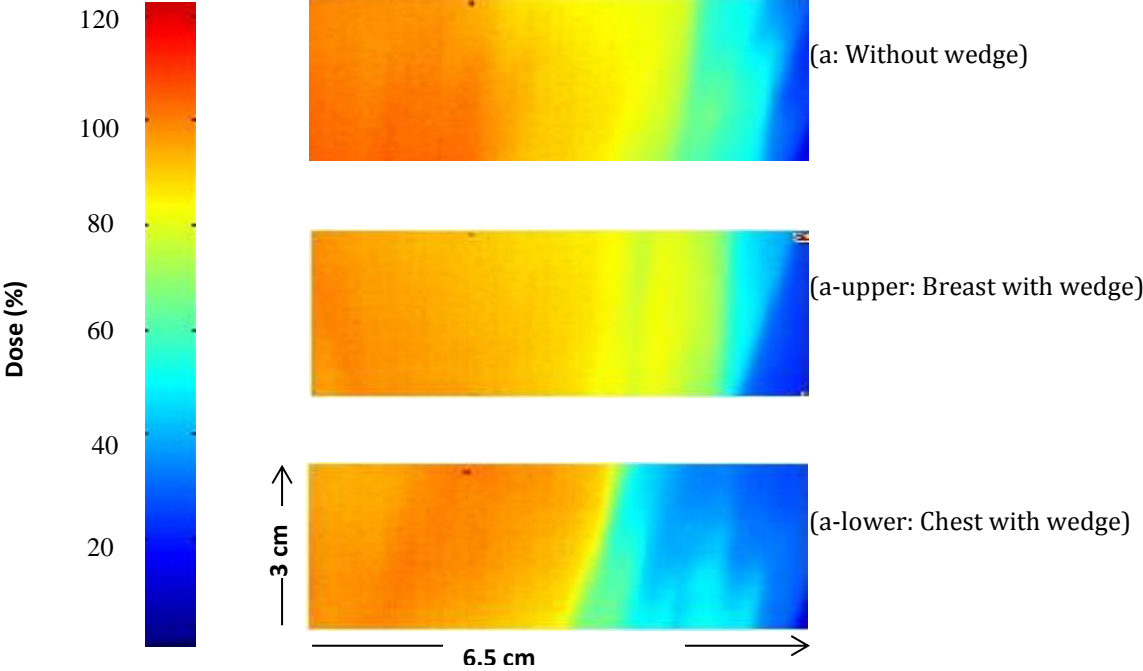


Figure 4.7: Measured dose profiles as determined by averaging the dose profiles along the Y-direction for each EBT3 film which presented in figure 4.6. Film in the skin fold without foam wedge (blue line), breast film with foam wedge (red dots), and chest film with foam wedge (green dash).

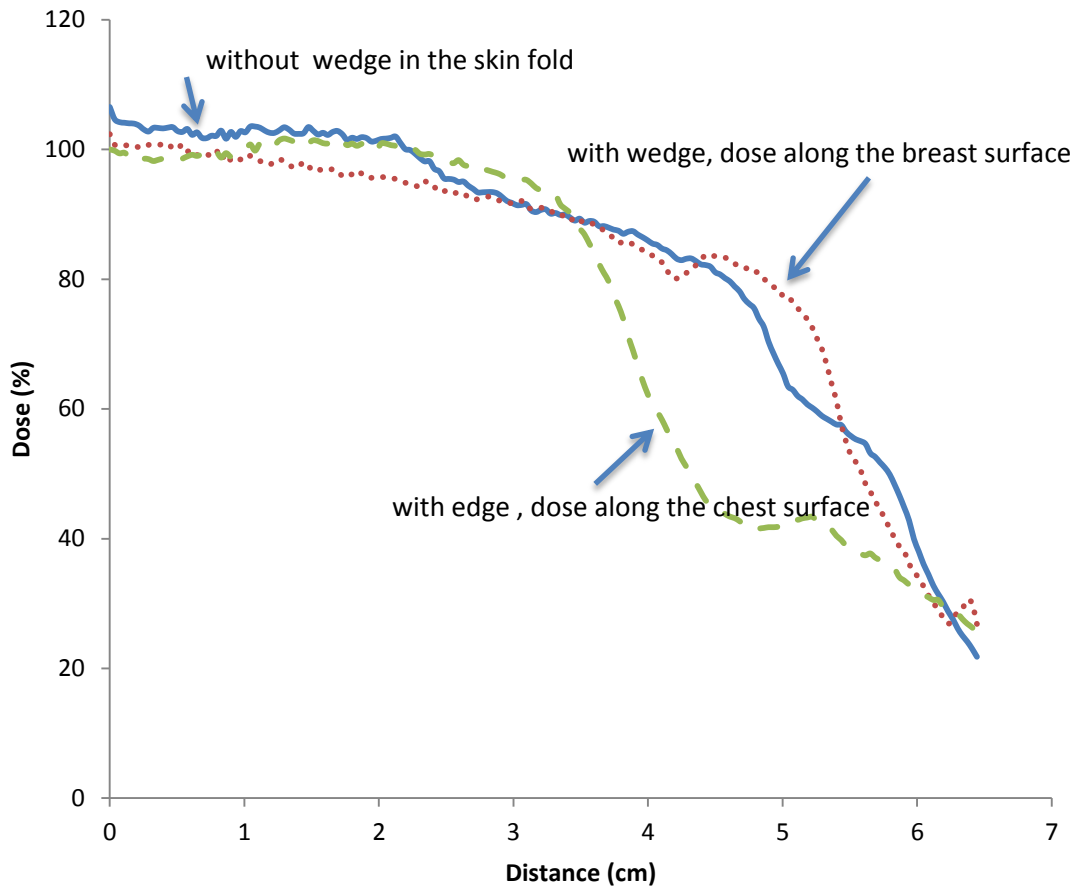
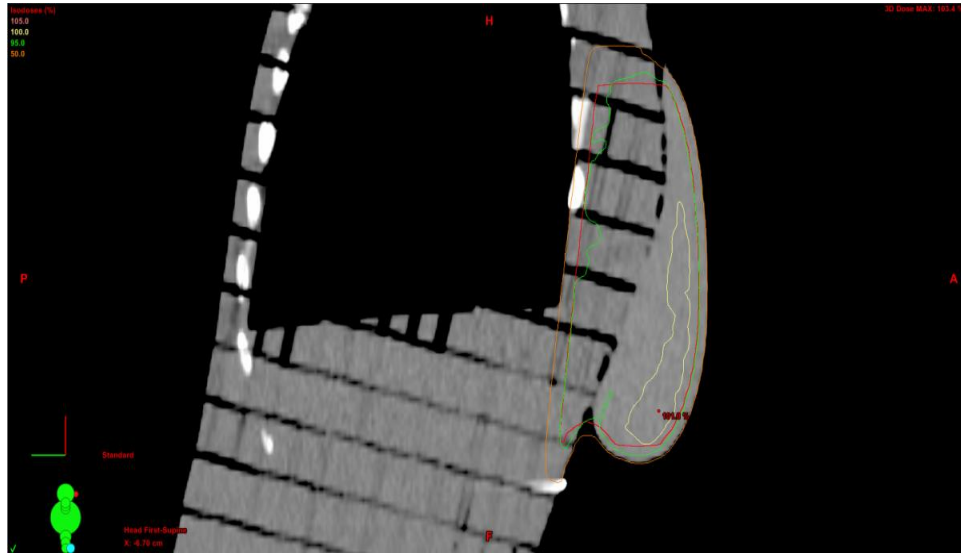


Figure 4.8: The difference in the dose distribution and water bag shape in without and with foam wedge plans in the sagittal view. Isodose lines: 100% in yellow line, 95% in green line, 50% in orange line, and PTV in red line.

(a) Without foam wedge.



(b) With foam wedge.

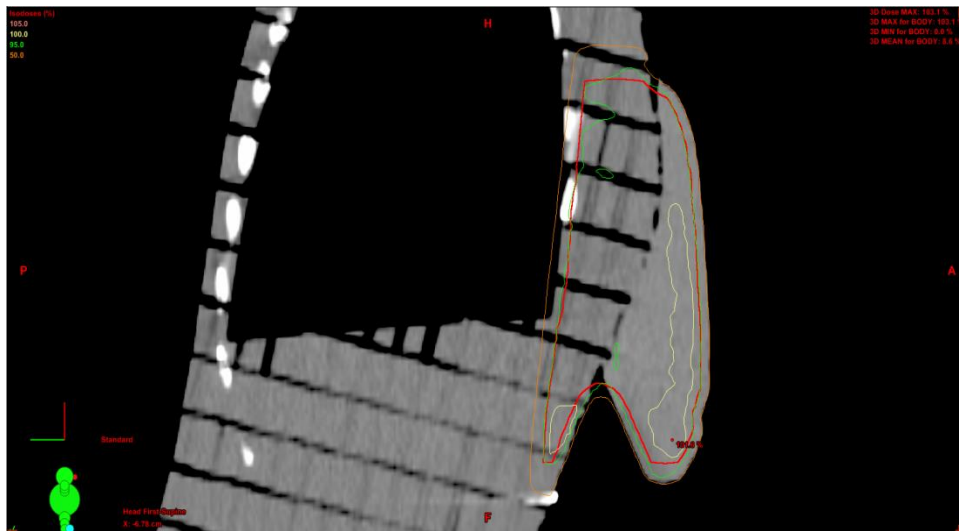


Figure 4.9: The entrance and exit dose measurements for (b: lateral), and (c: medial) films as shown in figures 4.2 and 4.3.

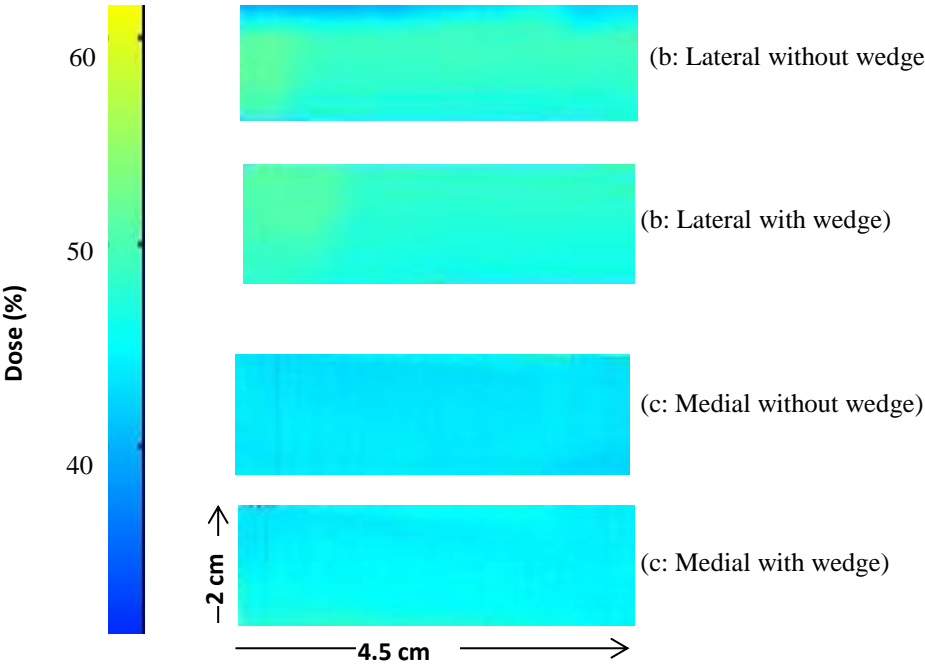
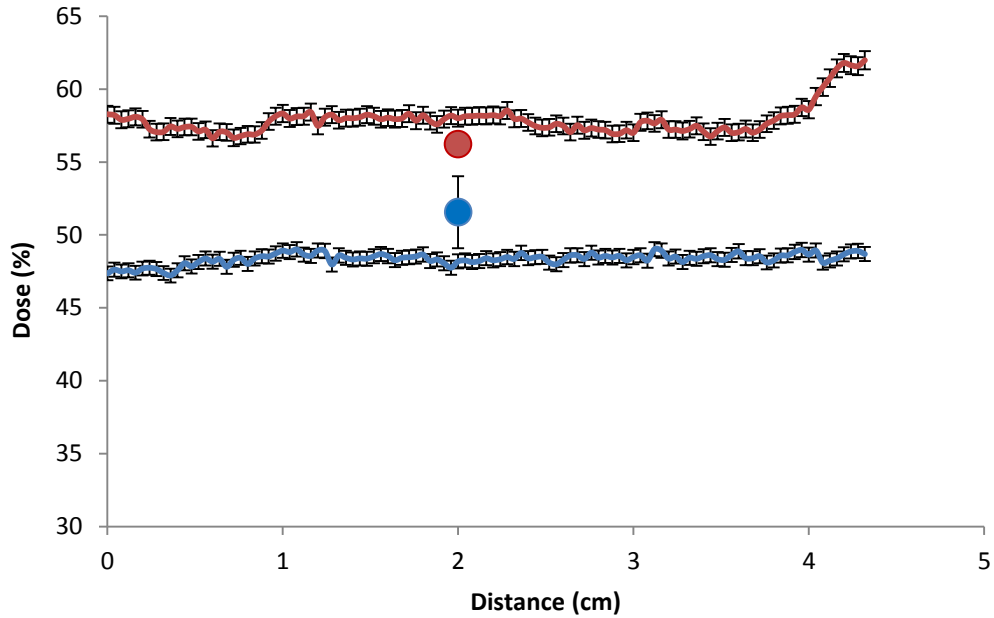


Figure 4.10: Illustration of the variation of the total dose from entrance and exit beams on medial and lateral sides of the water bag: medial (blue line) and lateral (red line) as presented in figure 4.9. For comparison, Eclipse point dose data (average of data in Table 4.1) is shown in the circles.

(a) Without wedge.



(b) With wedge.

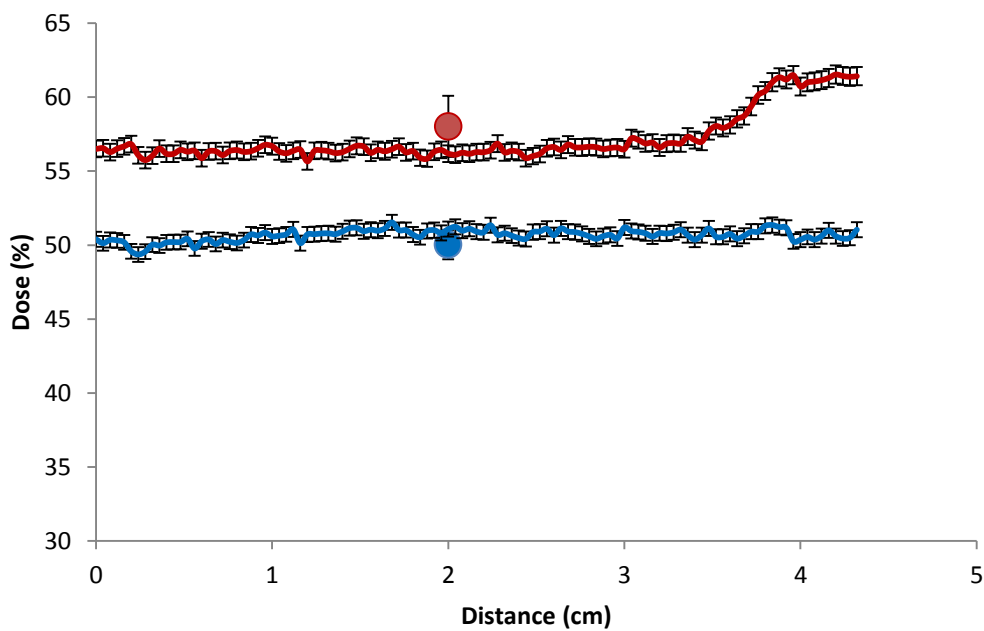


Figure 4.11: The comparison of Eclipse calculated skin dose vs. separation in ROI data from chapter 2(triangles), PROI data from chapter 3(circles), and data averaged over a 3 cm length on the lateral film on the breast phantom in this chapter (square).

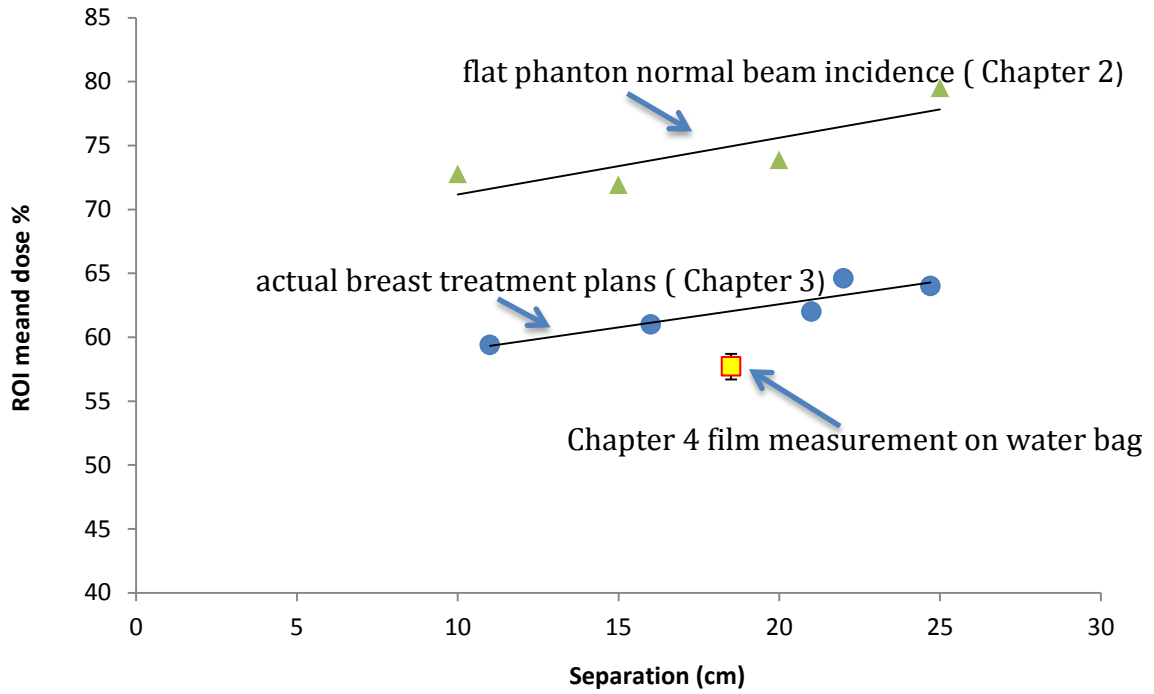
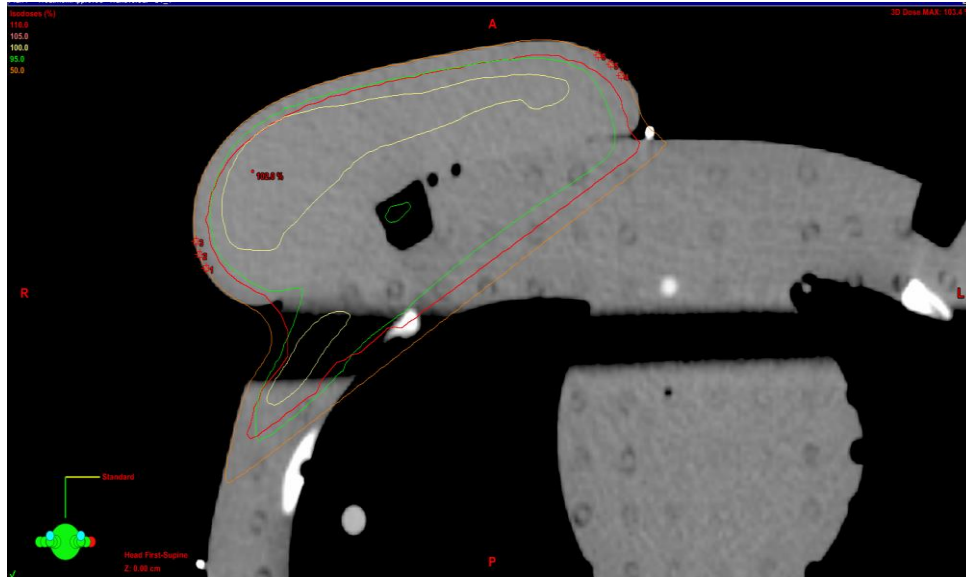


Figure 4.12: Cross sectional view of dose distribution and dose points for:

(a) Without foam wedge.



(b) With foam wedge.

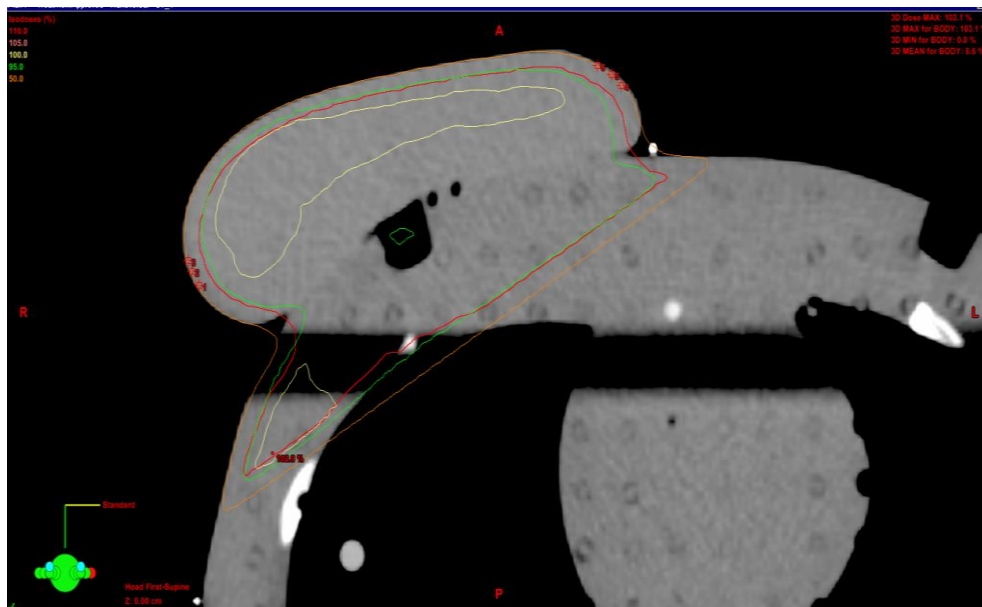


Table 4.1: Point's dose calculated by Eclipse TPS.

Points dose for without foam wedge plan (%)				
Point 1	Lateral	56.1	Medial	50.9
Point 2		56.6		49.5
Point 3		55.9		54.3
Points dose for with foam wedge plan (%)				
Point 1	Lateral	60.2	Medial	53.5
Point 2		56.1		48.4
Point 3		57.8		48.2

Chapter 5: Radiological properties for breast immobilization devices

5.1 Introduction

Skin reactions caused by the presence of skin folds are of concern in breast radiotherapy, as discussed in chapter 1, section 1.4.2. A suitably designed breast immobilization device should reduce skin folds and improve breast positioning, potentially leading to fewer side effects in radiation therapy of the breast. A challenge in the design of a suitable breast positioning device is the choice of construction material. The material must be rigid enough to support the weight of the breast (up to ~ 1 kg) without adversely affecting the skin dose by creating dose buildup. The literature review presented in chapter 1 identified several materials that have been investigated for this purpose. None of the materials presented was able to provide the combination of support and radiation translucence required for an effective device.

This chapter will focus on the radiological properties of carbon fibre for 6 MV and 10 MV photon beams. Comparison is made between dose buildup characteristics of carbon fibre sheet, solid water and the Styrofoam (Dow Styrofoam SM Insulation, Convoy Supply, and www.convoy-supply.com) material currently in use for breast positioning at the BCCA. Dose measurements were performed using a Marcus parallel plate ionization chamber as well as radiochromic film.

5.2 Methods and materials

5.2.1 Dose buildup curves: Marcus ionization chamber

The carbon fibre material studied was 1.219 g/cm³ density, and sheet thickness 0.03 cm (Prepreg 3K, Fibre Glast Developments Corp, and www.fibreglast.com). The Styrofoam (Dow Styrofoam SM Insulation, Convoy Supply, and www.convoy-supply.com) was density 0.03 cm³ and sheets were manually cut using a band saw.

Central axis depth-ionization measurements were performed using solid water phantom slabs, carbon fibre sheets, or low-density Styrofoam sheets as buildup material. The Marcus ionization chamber was placed at the central axis of the field with fixed SAD of 100 cm, 10x10 cm field size and 6 or 10 MV photon beams from a Varian CLIX linear accelerator (Varian Medical Systems, Palo Alto CA). 15 cm of backscattering material (solid water slabs) was used below the ionization chamber. All Marcus chamber ionization measurements were corrected using the accepted correction factors as a function of depth. The set up for the three experiments are shown in figure 5.1(a), 5.1 (b), and 4.1(c). An electrometer was used for ionization chamber readings.

Dose buildup curves were measured using depths of solid water from 0 cm to 5 cm, depths of carbon fibre from 0 cm to 0.3 cm of, and depths of low-density Styrofoam from 0 to 30 cm. For each depth the ionization measurement was performed for three irradiations delivering 300 mu each and then the average ionization value was acquired. All measurements were normalized to the ionization reading taken at d_{\max} in solid water. D_{\max} was 1.5 cm for the 6 MV beam and 2.6 cm for the 10 MV beam.

5.2.2 Radiochromic film dosimetry for Carbon fibre sheet

EBT3 GafChromic™ film (Ashland, NJ) dosimetry was performed to provide information on the variation in surface dose under carbon fibre sheet. Five Gafchromic™ film pieces were extracted from a single EBT3 Gafchromic™ film sheet. A small triangle cut was made in top right in of each film to indicate the orientation of the original. The film pieces were 5 cm x 9 cm in size.

From one carbon fibre sheet to seven sheets of carbon fibre were placed atop a 15 cm thick solid water phantom and irradiated using a 6 MV photon beam. A piece of EBT3 Gafchromic™ film was placed between the carbon fibre sheet and the solid water. For each measurement, an irradiation of 300 mu was delivered. The beam incident axis was perpendicular to the axis of the film. Each film dosimeter was irradiated individually. Film measurements were normalized to the film measurement at d_{\max} in solid water. Film scanning and digitization is as described in section 4.2.4

5.3 Results

5.3.1 Dose buildup using Marcus ionization chamber

Figures 5.2 and figure 5.3 show the three depth dose curves measured with the Marcus chamber in solid water, carbon fibre, and blue Styrofoam. All measurements were normalized to the dose at d_{\max} in solid water at 1.5 cm for 6 MV and 2.6 cm for 10MV. The minimum thickness of solid water available for these measurements was 2mm, thus finer depth resolution in solid water was not feasible. The surface dose measured using the Marcus chamber without any overlying absorber was 26.3% for 6 MV and 10 % for 10 MV.

The dose build-up in solid water and carbon fibre are identical, within experimental error, over the measured range of 10 sheets of carbon fibre for both 6 MV and 10 MV. The effective point of measurement of the Marcus chamber taken at the inner surface of the front electrode is 0.0023 cm. Marcus data was corrected for wall in-scattering using the same formula as applied in chapter 2. The dose with Marcus parallel plate ionization chamber was found to be 35.7 % of the dose to d_{\max} under 0.03 cm of carbon fibre (one sheet), 42.9 % at 0.06 cm (two sheets), increasing to 73.5 % at 0.3cm (10 sheets) for 6 MV, and 24.5 % at 0.03 cm (one sheet), 29.5 % at 0.06 cm (two sheets), increasing to 56.2 % at 0.3cm (10 sheets) for 10 MV.

The dose buildup in Styrofoam is dramatically different in comparison to solid water for both energies. Styrofoam build-up curve for 6 MV demonstrates a leveling off in dose at 72.7 % of the maximum dose in solid water starting at a depth of ~22 cm in Styrofoam. For 10 MV the dose buildup curve levels off at ~ 57.7% of the dose at d_{\max} in solid water at ~ 29 cm. Dose under 1cm of Styrofoam was 32.6% of the dose maximum in solid water for 6MV and 24.4% of the dose maximum in solid water for 10 MV.

5.3.2 Radiochromic film dosimetry for Carbon fibre sheet

Figure 5.4 shows carbon fibre film results converted to dose. A random variation (noise) of approximately +/- 1% is observed in the film data, consistent with the variation seen in chapter 3. There is no significant impact of the carbon fibre sheet weave pattern. The data demonstrates that the dose increases with increasing carbon fibre thickness and is consistent with the Marcus chamber results. The presence of increasing carbon fibre material thickness from 0.03 cm to 0.21 cm caused an increase in the surface dose

approximately 43.7 cGy to 88.7 cGy, respectively. The effective point of measurement of the film is the midpoint of the film adding an offset in depth of 0.14 mm to the measurement. The depth corrected film data averaged over the extent of the film is shown on figures 5.2 and 5.3 for direct comparison to the Marcus chamber data.

5.4 Discussion

Several studies have demonstrated that the use of breast immobilization increases the surface dose when compared to the non-immobilized breast (as mentioned in section 1.6). It has been suggested that maintaining skin dose below ~80% of the prescribed dose will significantly decrease the incidence of moist desquamation in breast cancer radiation therapy. In order to maintain the skin dose below 80% of the prescribed dose to the breast, an ideal breast support device should not increase surface dose by more than ~30%. This observation is based on the results of chapters 3 and 4, which demonstrated that the average dose over the first 3 mm of skin on the entrance and exit surfaces is approximately 50 to 60% of the prescribed dose.

The primary type of photon interaction in 6 MV and 10 MV x-ray beams is the Compton interaction. Compton is independent of atomic number (Z) and depends only on the number of electrons per gram (electron density). Also, as the photon energy increases, the Compton effect decreases (Johns & Cunningham, 1983, Page 155). The carbon fibre sheet density is 1.2 g/cm^3 , solid water density is 1.02 g/cm^3 , and Styrofoam is 0.03 g/cm^3 . Hence, in carbon fibre, slightly more dose buildup may occur in comparison with solid water. However, the carbon fibre sheet is somewhat porous and the measured data indicate that within experimental error, the dose buildup in carbon fibre sheet is the same

as in solid water. On the other hand, Styrofoam density is much lower than both the carbon fibre and the solid water density. Minimal dose buildup takes place in Styrofoam and minimal surface dose enhancement is seen.

Both carbon fibre and Styrofoam are found to be suitable materials for constructing a device for breast cancer treatment if the increase in dose buildup is considered in the device design. The presented data demonstrates that Styrofoam has the advantage of not increasing the surface dose if we can use less than one centimeter of Styrofoam. However, Styrofoam is not structurally robust for multiple uses, and is not easily cleaned. Three sheets of carbon fibre will increase the surface dose by ~20% for 6 MV photons and < 20% for 10 MV photons. In contrast to Styrofoam, heat cured carbon fibre sheet has the stiffness, and high tensile strength for constructing a device which can be reused many times and may be easily cleaned.

5.4 Conclusion

Considering all of the above, it is recommended that a breast immobilization device could be constructed of carbon fibre sheets using up to 3 sheets, or a combination of Styrofoam core of up to 1 cm thickness and carbon fibre exterior consisting of up to 3 sheets. The increase surface dose associated with this design should be clinically acceptable.

Figure 5.1 (a-c): Marcus ionization chamber measurement set up. 6 MV and 10 MV x-ray photon beams are used with 10×10 cm² field size, 15 cm of solid water as a back scatter.

(a) Solid water build up.



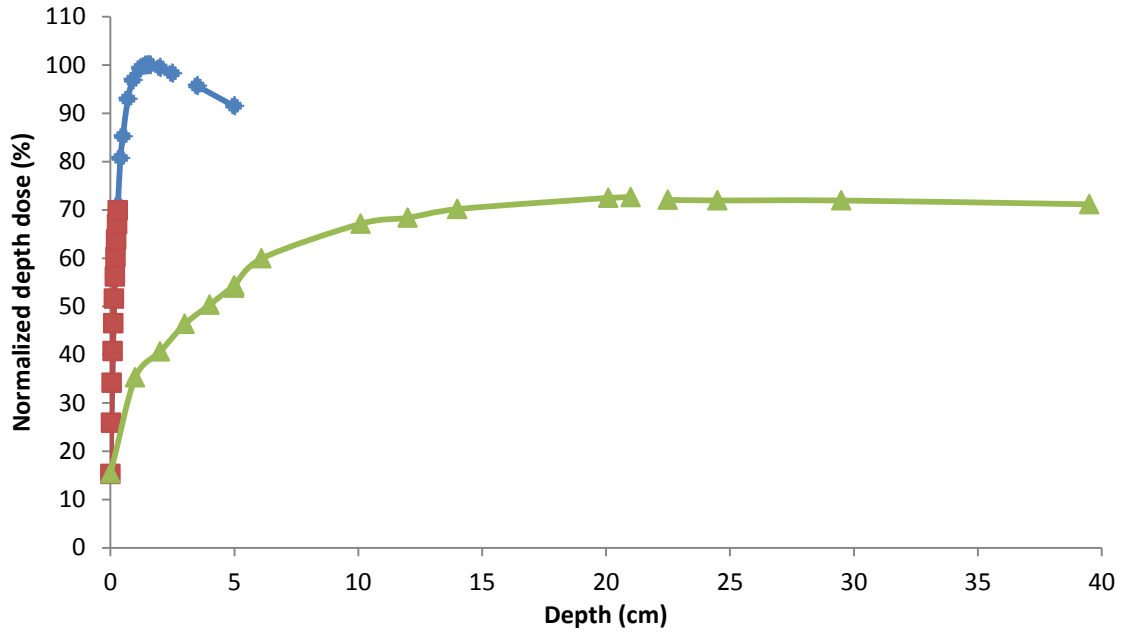
(b) Foam build up.



(c) Carbon fibre build up.



Figure 5.2: Build up curves for solid water (blue line), carbon fiber (red line), and Styrofoam (green line) using Marcus ionization chamber for 6 MV photon beam and with 10×10 cm² field size.



Maximized view (first 1 cm):

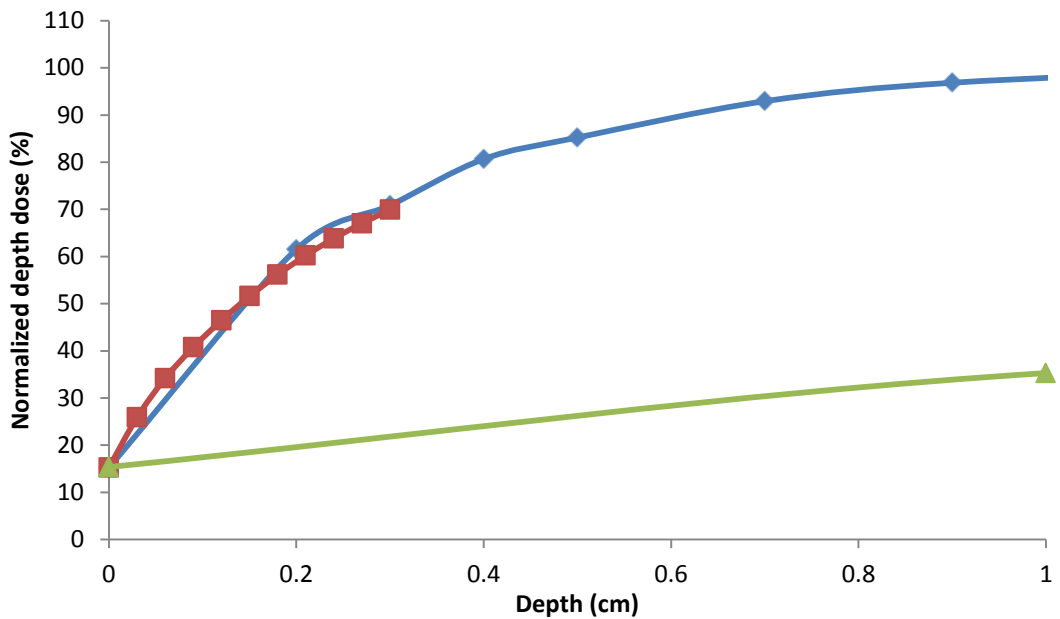
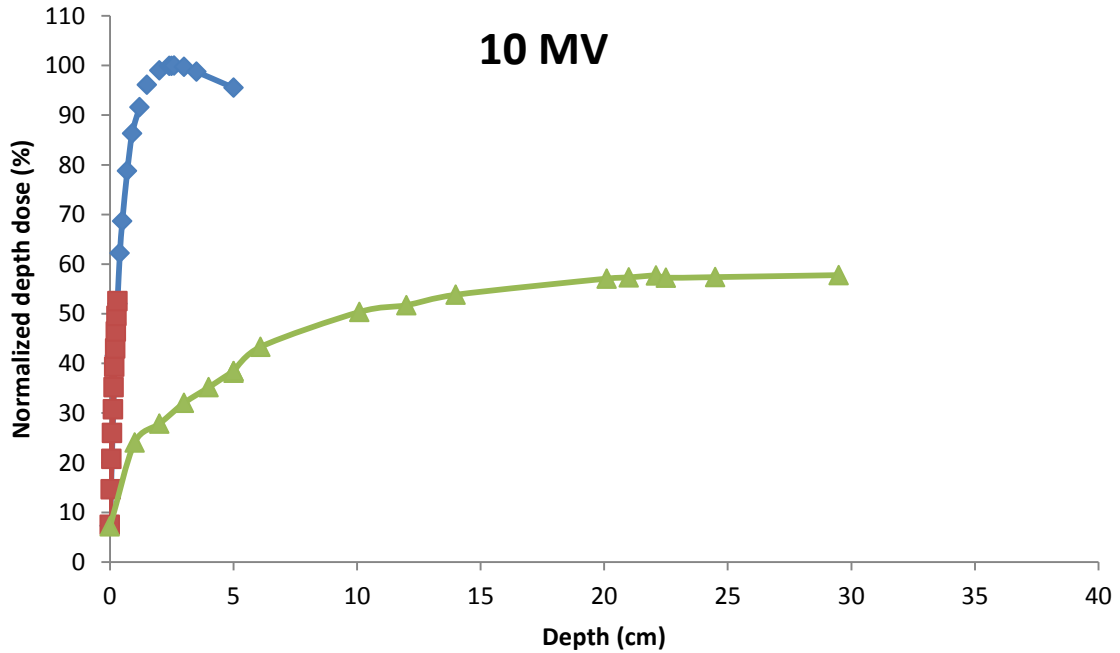


Figure 5.3: Build up curves for solid water (blue line), carbon fiber (red line), and Styrofoam (green line) using Marcus ionization chamber for 10 MV photon beam and with 10×10 cm² field size.



Maximized view (first 1 cm):

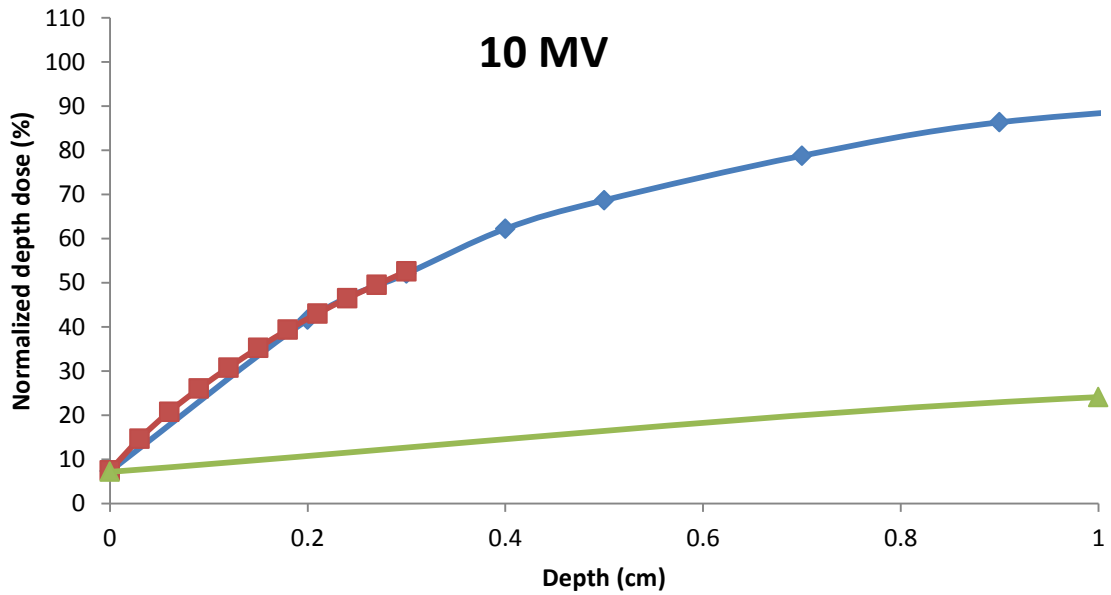
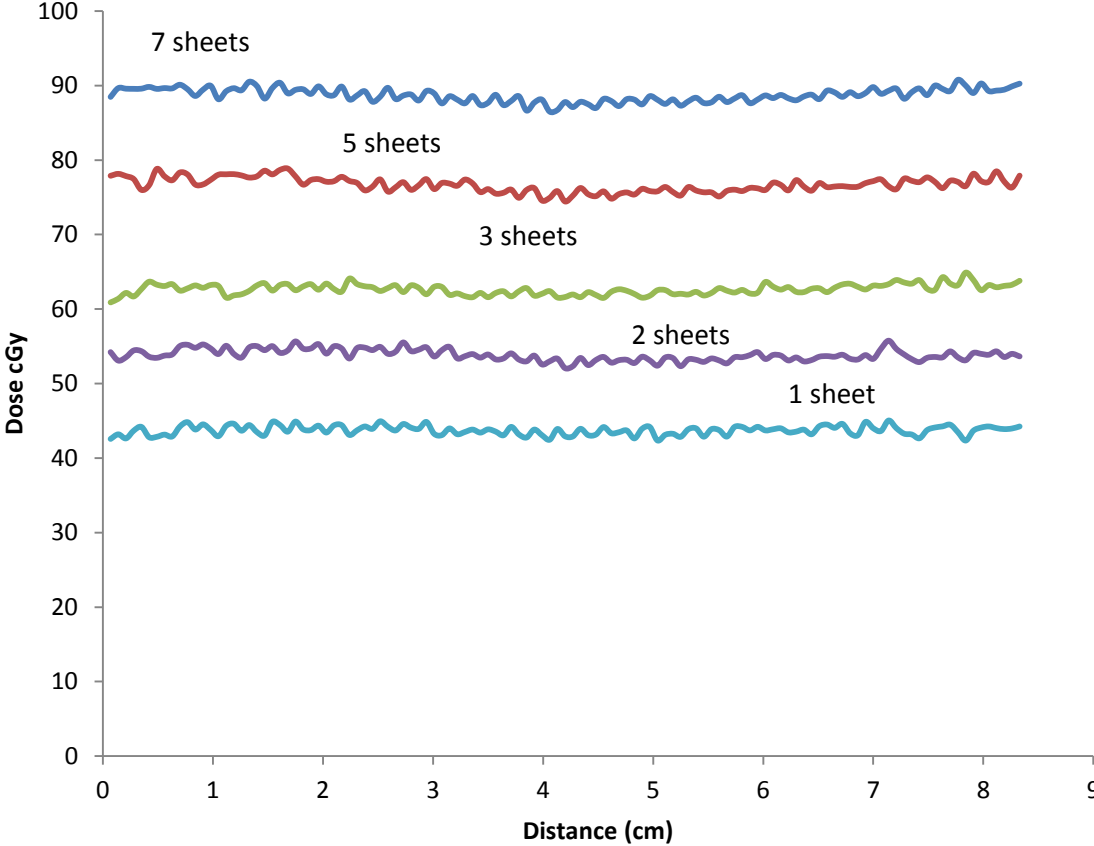


Figure 5.4: The variation of dose profiles for one-seven carbon fiber sheets measured by EBT3 films.



Chapter 6: Conclusion and future work

6.1 Conclusions

The work in Chapter two demonstrates that in megavoltage x-ray therapy, skin dose on medial and lateral breast surfaces can be expected to be less than 80% of the prescribed dose to the breast. In skin folds however, the skin receives 100% of the prescribed dose. In Chapter 3 a dosimetric study of a simple foam wedge breast positioning device, compared with an ideal breast positioning strategy, indicates that there is potential to improve skin dose and reduce the volume of normal tissue being irradiated beyond what is currently being achieved. To aid in further development of a suitable breast positioning device, it was demonstrated in Chapter 4 that EBT3 GafChromic™ film (Ashland, NJ) is a suitable dosimetric tool to characterize skin dose in breast radiation therapy. The results of Chapter 5 indicate that both Styrofoam and carbon fibre sheet may be suitable materials for the construction of a breast positioning device from a radiological perspective.

6.2 Future work

Work is underway at BC Cancer Agency to design a device which will enable better breast positioning, reduced skin and normal tissue dose, with more reproducible results, and will reduce patient setup time during therapy. The choice of the material to use for the proposed device is supported by the results of the carbon fibre characterization performed in this work. Evaluation of this device will first be performed in phantom then in a clinical trial. Ultimately the use of such a device is expected to improve the quality of life for breast cancer patients particularly those with skin folds.

References

1. Almberg, S. S., Lindmo, T., & Frengen, J. (2011). Superficial doses in breast cancer radiotherapy using conventional and IMRT techniques: A film-based phantom study. *Radiotherapy and Oncology*, 100(2), 259-264.
2. Arenas, M., Hernández, V., Farrús, B., Müller, K., Gascón, M., Pardo, A., et al. (2014). Do breast cups improve breast cancer dosimetry? A comparative study for patients with large or pendulous breasts. *Acta Oncologica*, 53(6), 795-801.
3. Barrett, A., Dobbs, J., Stephen, M., & Tom, R. (2009). *Practical radiotherapy planning*. London: Arnold.
4. Bentel, G. C., & Marks, L. B. (1994). A simple device to position large/flaccid breasts during tangential breast irradiation. *International Journal of Radiation Oncology, Biology, Physics*, 29(4), 879-882.
5. Bentel, G. C., Marks, L. B., Whiddon, C. S., & Prosnitz, L. R. (1999). Acute and late morbidity of using a breast positioning ring in women with large/pendulous breasts. *Radiotherapy and Oncology*, 50(3), 277-281.
6. Breast cancer in Canada Retrieved 2015 July 16, from <http://www.cbcf.org/ontario/AboutBreastCancerMain/FactsStats/Pages/Breast-Cancer-Canada.aspx>
7. Breast cancer society of Canada - statistics Retrieved 2015 July 14, from <http://www.bcsc.ca/p/46/l/505/t/Breast-Cancer-Society-of-Canada---Statistics>

8. Breast cancer statistics - canadian cancer society Retrieved 2015 July 14, from <http://www.cancer.ca/en/cancer-information/cancer-type/breast/statistics/?region=bc>
9. Chen, G., Liu, F., White, J., Vicini, F., Freedman, G., Arthur, D., et al. (2015). A planning comparison of 7 irradiation options allowed in RTOG 1005 for early-stage breast cancer. *Medical Dosimetry*, 40(1), 21-25.
10. Chen, X., Gilkeson, R. C., & Fei, B. (2007). Automatic 3D-to-2D registration for CT and dual-energy digital radiography for calcification detection. *Medical Physics*, 34(12), 4934-4943.
11. Cross, M. A., Elson, H. R., & Aron, B. S. (1989). Breast conservation radiation therapy technique for women with large breasts. *International Journal of Radiation Oncology, Biology, Physics*, 17(1), 199-203.
12. De Langhe, S., Mulliez, T., Veldeman, L., Remouchamps, V., van Greveling, A., Gilsoul, M., et al. (2014). Factors modifying the risk for developing acute skin toxicity after whole-breast intensity modulated radiotherapy. *BMC Cancer*, 14(1), 711.
13. Gerbi, B. J., Meigooni, A. S., & Khan, F. M. (1987). Dose buildup for obliquely incident photon beams: Technical reports: Dose buildup for obliquely incident photon beams. *Medical Physics*, 14(3), 393-399.
14. Gray, J. R., et al. (1991). Primary breast irradiation in large-breasted or heavy women: Analysis of cosmetic outcome. *International Journal of Radiation Oncology, Biology, Physics* 21.2, 347-354.
15. Gray, R., Early Breast Canc Trialists Collab, & Early Breast Cancer Trialists' Collaborative Group (EBCTCG). (2011). Effect of radiotherapy after breast-

conserving surgery on 10-year recurrence and 15-year breast cancer death: Meta-analysis of individual patient data for 10 801 women in 17 randomised trials.

Lancet, Elsevier Science INC, New York , 378(9804), 1707-1716.

16. Hopewell, J. W. (1990). The skin: Its structure and response to ionizing radiation. *International Journal of Radiation Biology*, 57(4), 751-773.
17. ICRP (International Commission on Radiological Protection). (1992). The biological basis for dose limitation in the skin No. ICRP Publication No. 59). Pergamon, Oxford:
18. ICRU (International Commission on Radiation Units and Measurements). (1999). Prescribing, recording and reporting photon beam therapy and measurements No. Report 62). Bethesda: MD: ICRU Johns, H. E., & Cunningham, J. R. (1983). The physics of radiology (4th ed.). Springfield, Ill: Thomas.
19. Johns, H. E., & Cunningham, J. R. (1983). The physics of radiology (4th ed.). Springfield, Ill: Thomas.
20. Keller LMM, Cohen R, Sopka DM, Li T, Li L, & Anderson PR. (2013). Effect of bra use during radiotherapy for large-breasted women: Acute toxicity and treated heart and lung volumes. *Pract Radiat Oncol*, 3(1), 9-15.
21. Kelly, A., Hardcastle, N., Metcalfe, P., Cutajar, D., Quinn, A., Foo, K., et al. (2011). Surface dosimetry for breast radiotherapy in the presence of immobilization cast material. *Physics in Medicine and Biology*, 56(4), 1001-1013.
22. Khan, F. M. (2003). The physics of radiation therapy (3rd ed.). Philadelphia, PA: Lippincott Williams & Wilkins.
23. Klein, E. E., & Purdy, J. A. (1993). Entrance and exit dose regions for a clinac-2100c. *International Journal of Radiation Oncology, Biology, Physics*, 27(2), 429-435.

24. Kraus-Tiefenbacher, U., et al. (2012). Factors of influence on acute skin toxicity of breast cancer patients treated with standard three-dimensional conformal radiotherapy (3D-CRT) after breast conserving surgery (BCS). *Radiation Oncology* 7.1, 217-.
25. Latimer, J. G., et al. (2005). Support of large breasts during tangential irradiation using a micro-shell and minimizing the skin dose--a pilot study. *Medical Dosimetry : Official Journal of the American Association of Medical Dosimetrists* 30.1, , 31-35.
26. López, E., Núñez, M. I., Guerrero, M. R., Moral, R. d., Dios Luna, J. d., Rodríguez, M. d. M., et al. (2002). Breast cancer acute radiotherapy morbidity evaluated by different scoring systems. *Breast Cancer Research and Treatment*, 73(2), 127-134.
27. Manoharan, S., & Pugalendhi, P. (2010). Breast cancer an overview. *Journal of Cell and Tissue Research*, 10(3), 2423.
28. Martincich, L., Bertotto, I., & Montemurro, F. (2012). Neoadjuvant therapy in breast cancer. *Imaging Tumor Response to Therapy*, 95-108.
29. Mayles, P., Nahum, A., Rosenwald, J. C., & Papanikolaou, N. (2007). *Handbook of radiotherapy physics: Theory and practice*. Boca Raton, FL: Taylor & Francis Group.
30. Metcalfe, P., Kron, T., & Hoban, P. (2004). *The physics of radiotherapy x-rays from linear accelerators (3rd ed.)*. Madison, Wis.: Medical Physics Pub.
31. Moody, A. M., Mayles, W. P. M., Bliss, J. M., A'Hern, R. P., Owen, J. R., Regan, J., et al. (1994). The influence of breast size on late radiation effects and association with radiotherapy dose inhomogeneity. *Radiotherapy and Oncology*, 33(2), 106-112.

32. Neal, A. J., et al. (1995). Correlation of breast dose heterogeneity with breast size using 3D CT planning and dose-volume histograms. *Radiotherapy and Oncology* 34.3, , 210-218.
33. Orton, C. G., & Seibert, J. B. (1972). Depth dose in skin for obliquely incident 60 co radiation. *The British Journal of Radiology*, 45(532), 271.
34. O'Shea, E., & McCavana, P. (2003). Review of surface dose detectors in radiotherapy. *Journal of Radiotherapy in Practice*, 3(2), 69-76.
35. Panettieri, V., Barsoum, P., Westermark, M., Brualla, L., & Lax, I. (2009). AAA and PBC calculation accuracy in the surface build-up region in tangential beam treatments. phantom and breast case study with the monte carlo code penelope. *Radiotherapy and Oncology*, 93(1), 94-101.
36. Peart, O. (2015). Breast intervention and breast cancer treatment options. *Radiologic Technology*, 86(5), 535M.
37. Quach, K. Y., Morales, J., Butson, M. J., Rosenfeld, A. B., & Metcalfe, P. E. (2000). Measurement of radiotherapy x-ray skin dose on a chest wall phantom. *Medical Physics*, 27(7), 1676-1680.
38. Salvo, N., Barnes, E., van Draanen, J., Stacey, E., Mitera, G., Breen, D., et al. (2010). Prophylaxis and management of acute radiation-induced skin reactions: A systematic review of the literature. *Current Oncology*, 17(4), 94-112.
39. Saur, S., & Frengen, J. (2008). GafChromic EBT film dosimetry with flatbed CCD scanner: A novel background correction method and full dose uncertainty analysis. *Medical Physics*, 35(7), 3094-3101.

40. Siegel, R. L., Miller, K. D., & Jemal, A. (2015). Cancer statistics, 2015. *CA: A Cancer Journal for Clinicians*, 65(1), 5-29.
41. Saur, S., Fjellsboe, L. M. B., Lindmo, T., & Frengen, J. (2009). Contralateral breast doses measured by film dosimetry: Tangential techniques and an optimized IMRT technique. *Physics in Medicine and Biology*, 54(15), 4743.
42. Siegel, R. L., Miller, K. D., & Jemal, A. (2015). Cancer statistics, 2015. *CA: A Cancer Journal for Clinicians*, 65(1), 5-29.
43. Sun, L., Huang, C., Chen, H., Meng, F., Lu, T., & Tsao, M. (2014). Using a thermoluminescent dosimeter to evaluate the location reliability of the highest-skin dose area detected by treatment planning in radiotherapy for breast cancer. *Medical Dosimetry : Official Journal of the American Association of Medical Dosimetrists*, 39(4), 348-353.
44. Torre, L. A., Bray, F., Siegel, R. L., Ferlay, J., Lortet-Tieulent, J., & Jemal, A. (2015). Global cancer statistics, 2012. *CA: A Cancer Journal for Clinicians*, 65(2), 87-108.
45. Van Gestel, D., van Vliet-Vroegindeweyj, C., Van den Heuvel, F., Crijns, W., Coelmont, A., De Ost, B., et al. (2013). RapidArc, SmartArc and TomoHD compared with classical step and shoot and sliding window intensity modulated radiotherapy in an oropharyngeal cancer treatment plan comparison. *Radiation Oncology*, 8(1), 37-37.
46. Verhey, L. J. (1995). Immobilizing and positioning patients for radiotherapy. *Seminars in Radiation Oncology*, 5(2), 100-114.
47. Von Essen, C. F. (1969). Radiation tolerance of the skin. *Acta Radiologica: Therapy, Physics, Biology*, 8(4), 311.

48. Zierhut, D., Flentje, M., Frank, C., Oetzel, D., & Wannemacher, M. (1994).

Conservative treatment of breast cancer: Modified irradiation technique for women with large breasts. *Radiotherapy and Oncology*, 31(3), 256-261.